University of Southampton

A frequency study of Sonoluminescence and Sonochemical Activity

By
Aurore Marie Léonore Vinçotte

A thesis submitted for the degree of
Master of Philosophy

Department of Chemistry

September 1999

UNIVERSITY OF SOUTHAMPTON

ABSTRACT

FACULTY OF SCIENCE

CHEMISTRY

Master of Philosophy

A FREQUENCY STUDY OF SONOLUMINESCENCE AND SONOCHEMICAL ACTIVITY

by Aurore Marie Léonore Vinçotte

The influence of the frequency of ultrasound on the transducer impedance, sound output, pressure field within the cell, degradation rates and light emission was investigated.

A Meldola blue solution was irradiated by ultrasound in a cylindrical glass cell over a range of frequencies from 20 kHz to 160 kHz. The variation in chemical rate was correlated with light emission (sonoluminescence) as a function of frequency. Sonoluminescence appeared to predict very precisely at which frequency chemical activity was the most efficient. Results obtained with Meldola blue degradation were confirmed by the study of another reaction, the oxidation of iodide into iodine.

Photographs taken during the sonication of a luminol solution were used to visualize the chemically active zone. Light patterns and local measurements of pressure within the cell were found to be consistent with a standing wave model with modal functionality. The pressure field, the audible sound output and the impedance of the transducer-cell-solution system gave through their frequency dependence, some indications of the chemical efficiency. However, they did not reflect the chemical activity as well as sonoluminescence.

Finally, for larger sonicated volumes, the overall rate constant of a particular reaction was found to be less important in agreement with the photon density of the respective cell.

Table of contents

Acknowledgements

I would like to thank Dr Peter Birkin for his supervision, his kindness, his attention and his patience to listen to my poor English.

Personal thanks to Laetitia, Fabrice and Stefano for all the hours of fun.

Thanks must also go to my parents for their financial support.

I would like to thank Dr J. Elliott, Dr G. Denuault and Dr G. Price for their last corrections.

List of symbols

Latin letters

a	The radius of the cell
A	Absorbance or Arrhenius prefactor
$A_n^{measured}$	The measured absorbance of the n^{th} sample
$A_n^{modified}$	Real absorbance of the n^{th} sample, see Appendix
c	Speed of sound
C	Concentration
D	Diffusion coefficient
E_a	Activation energy
f	Frequency
F	Faraday constant
I, i	Current
i_{ss}	Steady-state current
$j_{0,a}$	Value of the Bessel function at the boundary conditions
k	Wave vector
k	Reaction rate
k_m	Mass transfer coefficient
k_r	Radial component of the wave vector
k_z	Axial component of the wave vector
l	The UV-cuvette length or litre
L	Height of liquid in the cell
MBCL	Multiple bubbles chemiluminescence
MBSL	Multiple bubbles sonoluminescence
n	Number of exchanged electron
P	Pressure
P_a	Acoustic pressure
P_A	Amplitude of the acoustic pressure
P_0	Hydrostatic pressure
p_g	Partial pressure of gas within a bubble

P_i	Internal pressure within a bubble
P_L	Pressure in the liquid
P_m	Pressure in the liquid at the moment of collapse
p_v	Vapour pressure
p_σ	Laplace pressure
ΔP	Tensile strength
ΔP_C	Tensile strength
q	Odd integer
q'	Integer
r	Radius
R	Ideal gas constant
R_0	Initial radius of a bubble
R_{max}	The maximum radius reached by a bubble during expansion
S	Surface of the electrode
t	Time
T	Period
T_{amb}	Ambient temperature
V	Applied voltage
$V_{resistor}$	Voltage amplitude of the resistor
V_{RMS}	Root mean square voltage
V_{sol}	Volume of the sonicated solution
V_{sample}	Volume of a sample
x_a	Particle displacement at time t
X_0	Amplitude of the displacement
Z	Impedance

Greek letters

ε	Extinction coefficient
ϕ	Phase shift
γ	Ratio of the heat capacity at constant pressure to constant volume
λ	Wavelength

ρ	Density of the medium
σ	Surface tension
ω	Angular frequency of the sound wave

1. Introduction

1.1 Ultrasound

1.1.1 Background

The proliferation of organic wastes and polluted effluents has become one of the most important problems chemistry has to solve. Hence, for many years, there has been considerable interest in effluent treatment and destruction of organic pollutants. This has led to the study of a wide range of techniques such as photo-oxidation [1], membrane filtration [2, 3], biological treatment [4] and electrochemical oxidation [5]. Irradiation by ultrasound also appears to efficiently destroy organic impurities. This latter technique is particularly attractive because it can be carried out under very mild conditions (room temperature, atmospheric pressure). This manuscript reports a study of a model chemical reactor and describes the factors affecting the efficiency of such a system.

1.1.2 History of ultrasound

The term 'ultrasound' refers to sound waves of a frequency above human hearing, that is above 20 kHz. The first investigations of ultrasound dates back ca. 120 years. In 1880, the Curie brothers discovered the piezoelectric effect and its inverse, which allowed the conversion of a mechanical motion into an electrical signal. When subjected to some external mechanical stress, some crystalline materials, such as quartz, develop an internal electric field. This effect is reversible: if external forces are removed, charges disappear. The inverse effect is used as the principle of modern transducers (ultrasonic sources). The first practical use of ultrasound was found by Galton using whistles made from a brass tube. Such whistles, emitting sounds of known frequencies, were used to investigate the threshold frequency of hearing for humans. However, it was not until the First World War that the first industrial application, the detection of enemy submarines (SONAR), was successfully applied.

An explanation of the physical properties of sound is now presented.

1.1.3 Transmission of a sound wave in aqueous media

Sound is a waveform that propagates away from a source in an elastic medium. Sound waves are classed as longitudinal, in that the displacement of particles is parallel to the direction of motion of the wave.

Vibration of the sound source provokes the motion of a layer of molecules in the medium. This layer is also compressed by the adjoining layer, so the contact forces applied to the second layer are modified and this layer is no longer in equilibrium. In this way, the motion is transmitted step by step. After collision the first layer returns to its initial position because of the rarefaction due to the motion of the sound source in the other direction. Hence, the displacement of a particle in such a medium is sinusoidal:

$$x_a = X_o \cos(\omega t) \quad (1)$$

where x_a, X_0, ω refer to the particle displacement at time t, the amplitude of the displacement and the angular frequency of the sound wave.

Hence, the disturbance caused by the source provokes a succession of compression and rarefaction regions. It is obvious to correlate a compression region (high population density) to high pressures and a rarefaction region (low population density) to low pressures. The motion of the sound source in a medium establishes a sinusoidal wave of acoustic pressure, both displacement and pressure variations occur along the axis of propagation wave, but they are out of phase by $\pi/2$ radians.

$$P_a = P_A \sin(\omega t) \quad (2)$$

where P_a is the acoustic pressure at time t and at a given point, P_A is the maximum acoustic pressure of the wave and ω is the angular frequency of the sound wave.

This acoustic pressure is superimposed on the atmospheric pressure. Hence, the pressure in the liquid is the sum of static and oscillating terms:

$$P_L = P_o + P_A \sin(\omega t), \quad (3)$$

$$P_{L,\,min} = P_o - P_A, \text{ during rarefaction phase,} \quad (4)$$

$$P_{L,\,max} = P_o + P_A, \text{ during compression phase.} \quad (5)$$

where P_L, $P_{L,\,min}$, $P_{L,\,max}$ and P_o refer to the pressure in the liquid, minimal pressure in the liquid, maximal pressure in the liquid and the hydrostatic pressure.

If the acoustic pressure amplitude is higher than the hydrostatic pressure, then the pressure within the liquid could reach negative values, when the liquid will be in tension.

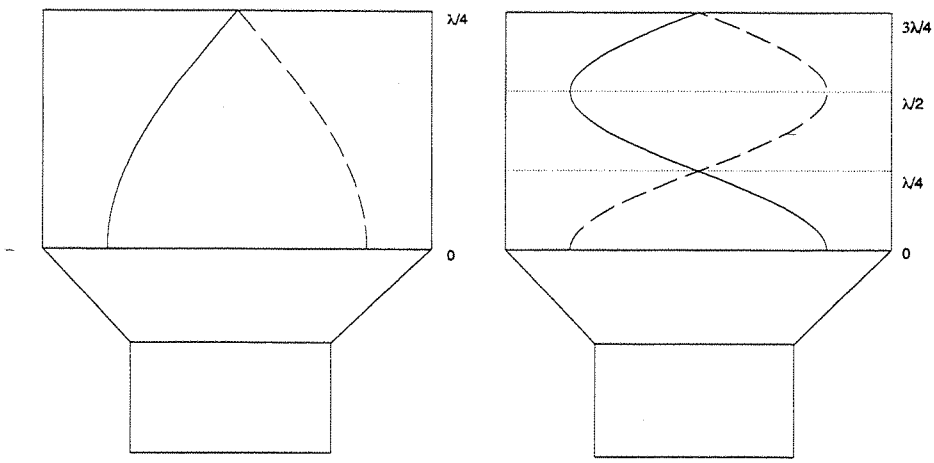

Figure 1.1: Simplistic model of 'standing waves pattern'. The figure shows the first two possible sound fields within the cell. Pressure minima are observed at the interface liquid/air.

When these sound waves reach an interface (liquid/glass cell or liquid/air), they are partly transmitted and partly reflected. Reflection under suitable length and frequency conditions leads to the formation of 'a standing wave pattern' caused by the interference between the incident and reflected waves. In this simplistic model shown in figure 1.1, areas where the pressure excersion is at a minimum are termed "pressure nodes" and can be observed at multiples of half wavelength distance from the interface (the interface

liquid/air is a pressure node). Conversely areas of maximum pressure ("pressure antinodes") occur at (2n+1)/4 λ positions through the system, where n = 1, 2, 3.... In such type of waves, energy is transmitted from one position to another, and they are therefore called 'progressive waves'. Energy is also lost within the medium in which it propagates. The energy loss is proportional to e^{-2bx}, where b, x represent a constant characteristic of the medium and the propagation length.

During the propagation of ultrasonic waves, creation and activation of gas bubbles, a process termed cavitation, may occur. In the next paragraph, this phenomenon will be outlined.

1.2 Cavitation

1.2.1 Nucleation, Growth and Collapse

Cavitation refers to the creation and the expansion of bubbles. Under suitable conditions, the final stage of cavitation can lead to the violent collapse of bubbles.

Cavitation effects were first studied by Sir John Thornycroft and Sidney Barnaby [6] in order to explain the poor performance of a destroyer propeller. They showed that this low efficiency was due to the creation of voids and clouds of bubbles when the lowest pressure around the blade dropped to a particular value.

1.2.1a Nucleation

One of the nucleation sites of cavitation can be found when a large number of minute gas bubbles are present. These bubbles do not diffuse because they are stabilized by organic impurities or 'skin' surrounding them [7]. Major weaknesses are found at the boundary between a liquid and a solid. This boundary can be either the wall of the cell or small contaminant particles within the liquid. Gas-vapour nuclei trapped in these crevices of a particle undergo a decrease of pressure making the liquid-gas interface more convex and can cause the formation of a bubble (Figure 1.2).

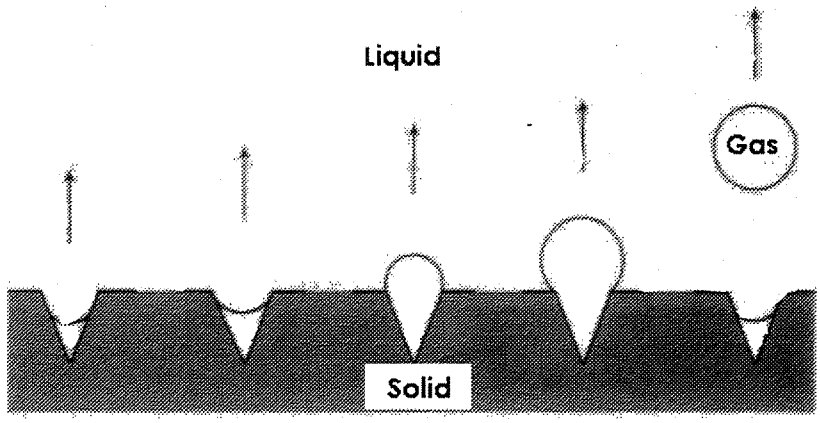

Figure 1.2: Bubble formation from a gas vapour nucleus trapped in a conical pit (after Young [7])

1.2.1b Stable and transient cavitation

Depending on the physical conditions (such as amplitude of the acoustic pressure, frequency of the driving force, temperature, nature of the solvent) two types of bubble behaviour have to be considered. In the first case, bubbles grow during the rarefaction phase and their size decreases during compression phase. This oscillating behaviour lasts during several acoustic cycles. This type of cavitation is called 'stable' or 'non-inertial' cavitation. In the second case, bubbles expand to at least twice their original size and subsequently collapse violently usually disintegrating into a mass of smaller bubbles (Figure 1.4). This type of behaviour is termed 'inertial' or 'transient' cavitation. The type of bubble behaviour will change as the acoustic pressure is modified, all other parameters remaining the same.

Internal pressure within a bubble is the sum of the pressure of dissolved gas and the pressure of liquid vapour

$$P_i = p_g + p_v \qquad (6)$$

When bubbles are in equilibrium with the surrounding fluid, the internal pressure is equal to

$$P_i = P_L + p_\sigma \tag{7}$$

where p_σ is the Laplace pressure or the surface tension pressure equal to $p_\sigma = 2\sigma/r$ (where σ is the surface tension of the liquid and r is the bubble radius).

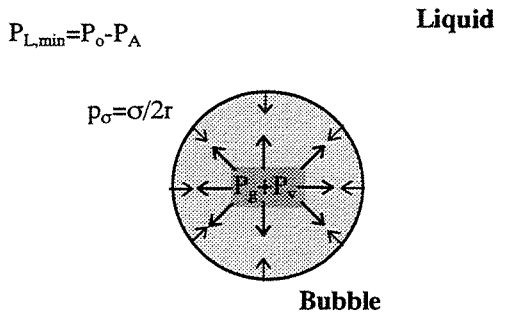

Figure 1.3: Forces exerced on a bubble within solution

The Laplace pressure, tends to maintain the gas within the bubble. To provoke the collapse of a bubble, the pressure in the liquid should counteract this cohesion force. Such a tension corresponds to the negative value of the pressure within the liquid when the amplitude of the acoustic pressure is higher than the hydrostatic pressure ($P_L=P_o+P_A \sin(\omega t)$). Once the bubble is larger than some critical radius the pressure balance (i.e. $P_o-P_A+2\sigma/r = p_g+p_v$) across the wall cannot be maintained, and the bubble will expand explosively.

Hence, the liquid will cavitate if the acoustic pressure

$$P_o - P_A + \frac{2\sigma}{r} < p_g + p_v \tag{8}$$

Thus, for the liquid to cavitate

$$P_A > P_o + \frac{2\sigma}{r} - p_g - p_v \tag{9}$$

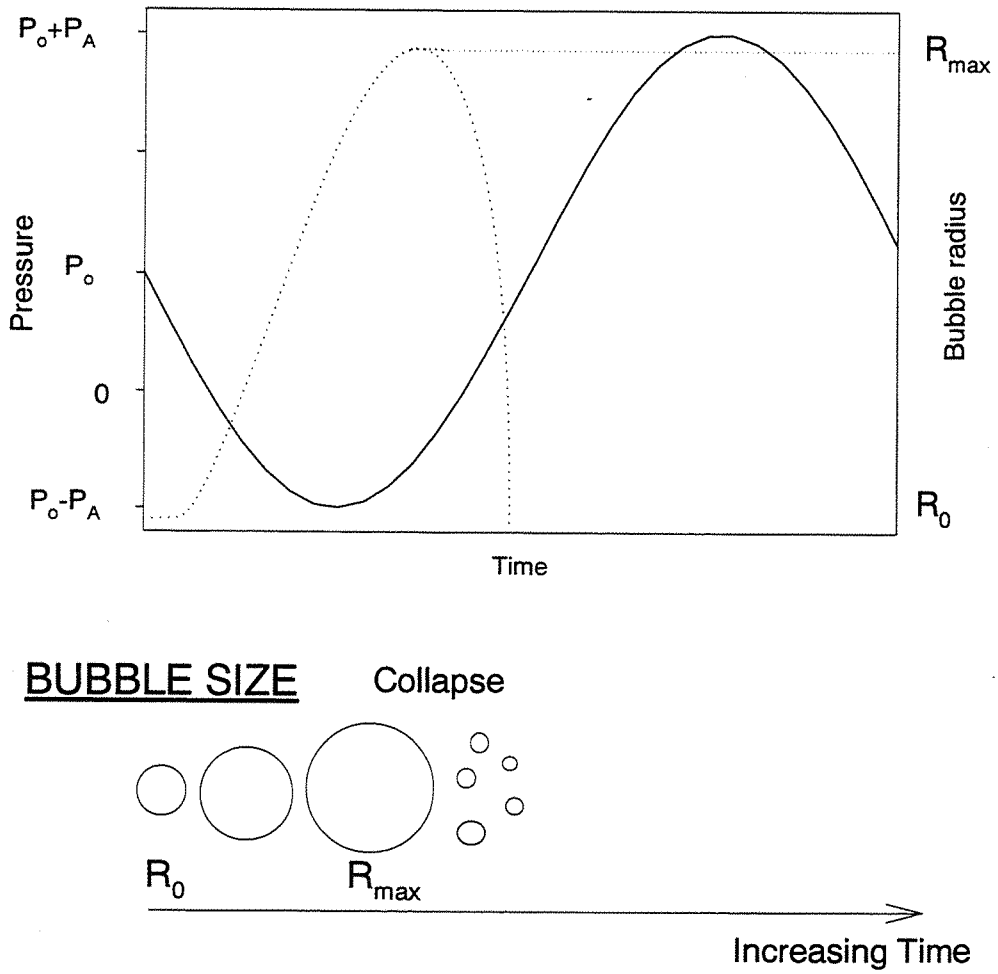

Figure 1.4: The figure shows the effect of pressure variation within a liquid on bubble size in the case of transient cavitation.

As stated previously, there is a fundamental difference between stable and transient cavitation. Passage from one behaviour to another occurs at a 'cavitation threshold'. Modification of several external parameters affects drastically the nature of bubbles and this threshold value.

1.2.2 Factors affecting cavitation

1.2.2a External pressure

An increase in external pressure provokes an increase in the hydrostatic pressure. Hence, cf. equation (9), the application of greater acoustic pressure and therefore intensities will be required to observe cavitation.

1.2.2b nature of the solvent

Cavitation is affected by the vapour pressure of the solvent: a solvent with a high vapour pressure is expected to cavitate at low acoustic pressure but produce relatively unenergetic cavitation. Suslick and coworkers [8] studied the effect of the solvent vapour pressure on ultrasound induced cavitation and found that decreasing the vapour pressure accelerated the reaction giving evidence that an increased bubble collapse energy enhanced sonochemical reaction rate.

1.2.2c Temperature

In general, increasing the temperature causes a reduction of the intensity threshold required to produce cavitation. This is probably due to an increase in the vapour pressure of the liquid [8]. Hence, an increase in temperature favours the nucleation phenomenon, but has an opposite effect on transient cavitation. As shown by Lorimer [9] the production rate of hydroxyl radicals (which is highly correlated to transient cavitation cf. § sonochemistry) is described by a modified Arrhenius equation:

$$\ln k = \ln A - \frac{E_a}{R(\gamma - 1)P_m} * \frac{P_v}{T_{amb}} \qquad (10)$$

where k, A, γ, E_a, R, P_m, P_v, T_{amb} represent the reaction rate, the Arrhenius prefactor, the ratio of heat capacity, the activation energy, the gas constant, the pressure in the liquid at the moment of collapse and the vapour pressure of the liquid.

The conclusion is that by decreasing the temperature, and hence the vapour pressure of the solvent, chemical activity can be enhanced.

These controversial effects are summed up in figure 1.5.

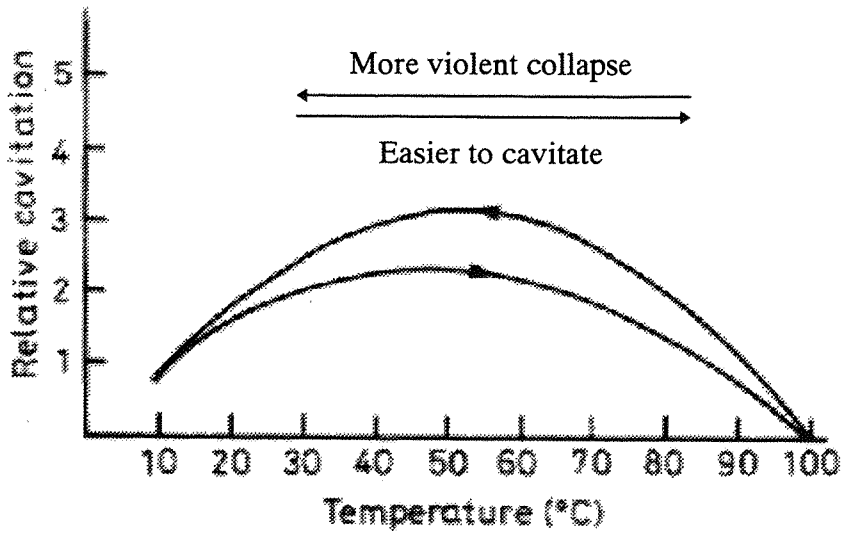

Figure 1.5: Effect of temperature on cavitation threshold in tap water and its associated hysteresis effect (after Kurtze [10])

1.2.2.d Dissolved gas

The nature and concentration of dissolved gases in a cavitating liquid significantly affect the mechanical and chemical effects of cavitation. The cavitation threshold increases when the solution is degassed. This phenomena can be explained by considering a nucleation bubble containing some gas. In this case the pressure is the sum of the partial pressure of this gas, p_g and the vapour pressure. Hence, the equilibrium pressure in the liquid is:

$$P_i = p_g + p_v - 2\frac{\sigma}{r} \qquad (11)$$

where P_i, p_g, p_v, σ and r represent the internal pressure within the bubble, the pressure of gas, the pressure of liquid vapor, the surface tension and the bubble radius.

The critical tension is:

$$\Delta p = p_v - P_i = 2\frac{\sigma}{r} - p_g \qquad (12)$$

Thus dissolved gases decrease the tensile strength.

However, solutes with a high thermal conductivity, like hydrogen, inhibit chemical reactions. Presumably gases with higher conductivities produce lower temperatures during the adiabatic compression of the bubbles.

1.2.2e Ultrasound intensity

It is obvious that by increasing ultrasonic intensity larger amplitudes of acoustic pressure are obtained. Hence, during rarefaction phases, constrain forces applied to bubbles are more important. Collapses are therefore more likely. The ultrasonic intensity can be increased to an upper limit. This limit depends on properties of the piezoelectric crystal and on the formation of bubble clusters. Damage to the piezoelectric components can be provoked if the forces applied to them become too large. Moreover an increase of the intensity (figure 1.6) leads to the formation of a bubble conglomerat at the pressure antinodes. A large number of bubbles causes the formation of larger and more stable bubbles.

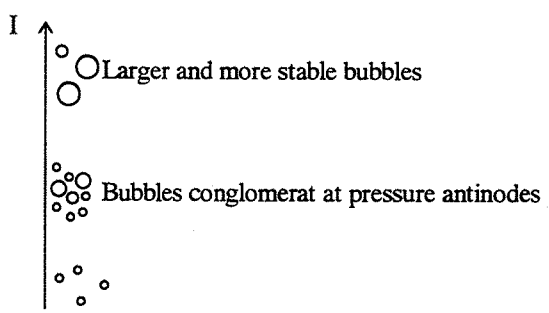

Figure 1.6: An increase of ultrasound intensity provokes the formation of a bubble conglomerat and then to larger and more stable bubbles

These clusters have another negative effect, they damp the sound energy as the wave propagates causing a decrease in the propagation of sound. In other words such a cloud of bubbles acts as a screen and reduces the amount of acoustic energy transmitted to the fluid.

1.2.2f frequency

As the frequency of the sound wave is increased the shorter the rarefaction cycle becomes. Time needed to create and grow a bubble is finite and it may be that the time available during a rarefaction cycle is too short to allow growth. Thus, as frequency increases a dramatic effect on the bubble growth can be seen (Figure 1.7).

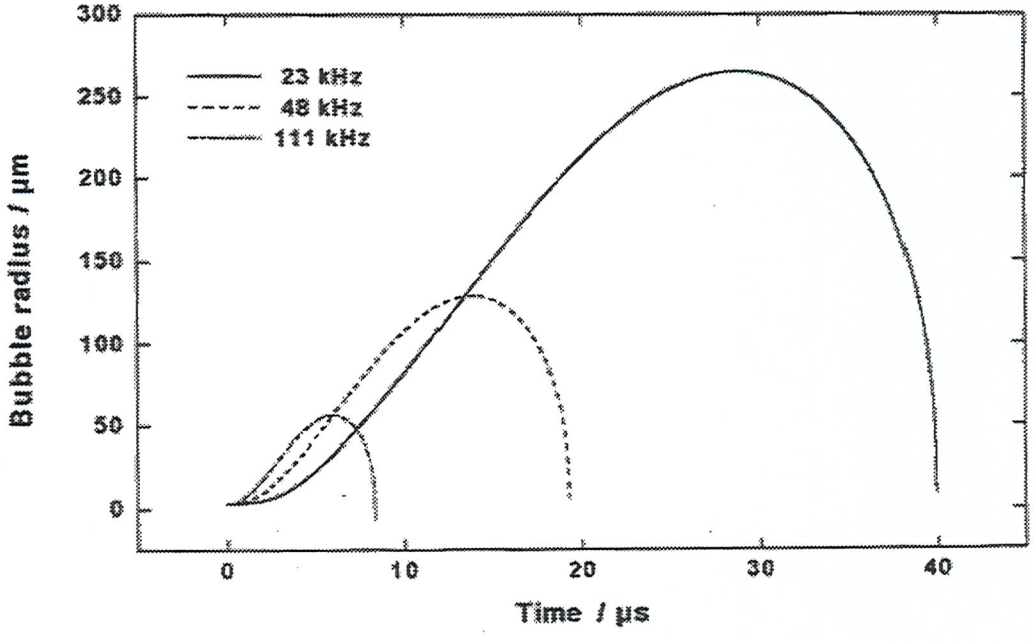

Figure 1.7: Effect of frequency on bubble growth (after Silva-Martinez [11])

However, as shown in figure 1.8 , this problem can be overcome by increasing ultrasound intensity, which gives more powerful rarefaction cycle.

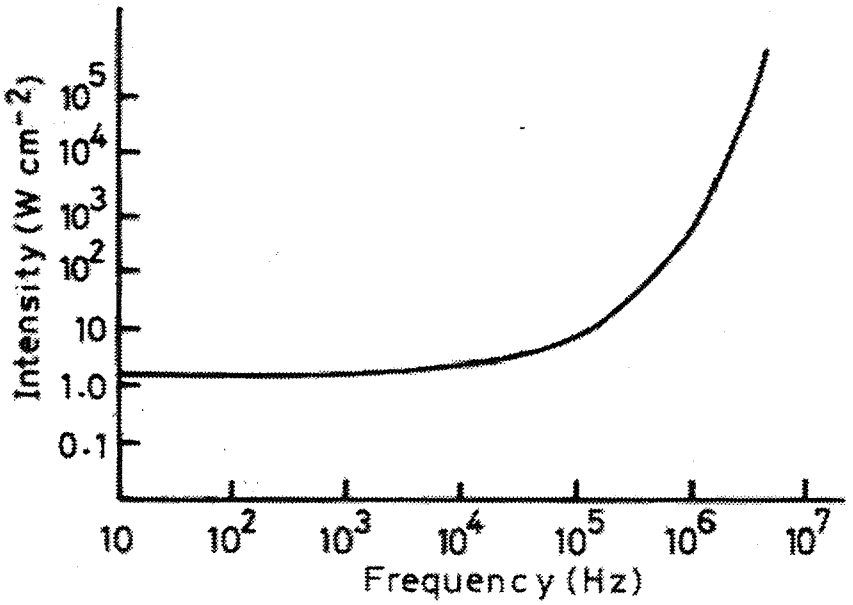

Figure 1.8: Effect of ultrasonic intensities on the cavitation threshold for degassed water at room temperature (after Perkins [12])

As can be seen on the plot, the intensity required to produce cavitation increases drastically above 100 kHz.

This study of acoustic cavitation is of particular interest, because, as described in the following paragraphs, most ultrasonic applications use the mechanical and chemical effects of cavitation.

1.3 Applications of ultrasound in daily life

Two types of ultrasound classed by their frequency ranges are commonly employed. High frequency ultrasound is mostly used for investigation, in detection or for analysis. At low frequency, a large range of tasks (such as cleaning, chemical reactivity modification, localised heating) can be performed using cavitation.

1.3.1 Detection

Measurement of the time lapse between emitting a sound and receiving an echo is the principle used for the detection under the sea (SONAR, SOund, Navigation And

Ranging) [13]. This technique is used in the fields of geography and geology for localisation of minerals and oil deposits and also as a depth gauge for seas and oceans.

1.3.2 Production of emulsion

Ultrasound can be used to emulsify two immiscible liquids. One liquid is slowly added to another, meanwhile ultrasound is applied to the second liquid. In such a way the added liquid rapidly breaks up into minute drops. These ultrasonically produced emulsions are used in the food, paint, cosmetic and pharmaceutical industries.
In emulsion processes ultrasound also can be used to characterize and to detect floculation [14].

1.3.3 Cleaning

The first use of ultrasound as a cleaning agent was performed in Germany during the Second World War. Cleaning is achieved by immersion of an object in a bath containing a suitable solvent, such as cyclohexane or trichloroethylene. Such a technique allows to wash cavities inaccessible with more common methods. Since bubbles tend to form preferentially in craks and crevices on particles or surfaces, their vibrations occur at the best place to clean the most inaccessible part of the object.

1.3.4 Working of metals

The method of ultrasonic pulse defectoscopy is used to test welded joints without breaking them [15]. Metal cutting can also be achieved by coupling a drill bit to a transducer in which ultrasonic oscillations are generated. The cutting is performed by an abrasive slurry that is placed between the drill bit and the workpiece. This method provides the possibility of obtaining very complicated shaped holes by making and using a bit with a cross section of the required shape.

1.3.5 Welding of plastics

Ultrasonic welding of plastics including sticking plastic to metal or inserting metal into plastic, is extremely widespread. The application of ultrasound to this task allows rapid and precise work. In this way heating of the surrounding parts is not induced. Moreover, using this method, plastics show a high joint strength that is equivalent to between 90-98% of the normal material strength.

1.3.6 The uses of ultrasound in food technology

T. J. Mason *et al.* [16] summarised two types of ultrasound which are used in industry:

- High frequency, low energy ultrasound in the MHz range
- Low frequency, high energy ultrasound in kHz range

Ultrasound was first used as an analytical technique to test the quality of food. An estimation of the degree of emulsification can be achieved by the measurement of velocity in conjunction with attenuation coefficients. The degree of creaming or settling can also be determined. Such information gives an indication of the stability of products such as fruit juices and mayonnaise.

Ultrasound, depending on its frequency, can also be used either to stimulate the activity of living cells and enzymes or to kill micro-organisms. In the first case, the production of food products is faster and gives higher yields. In the second case, ultrasound can be employed in conjunction with another technique (bactericide, heating). As an example a combination of heating and irradiation by ultrasound enables the reduction of the heating time required for pasteurisation and sterilisation of milk.

Cell disruption and effective mass transfer provoked by mechanical effects of ultrasound are also known to be very useful in the extraction of organic compounds contained within the body of plants. In such a way the extraction of sugar from sugar beet is achieved [17].

Crystallisation and freezing time can be reduced under sonication conditions. It is thought to play a number of roles in the initiation of seeding and subsequent crystal formation and growth.

1.3.7 The uses of ultrasound in medicine and in dentistry

Ultrasound was first used in medicine (1930's) as an alternative for massage.

Ultrasonic pulse echo techniques provide informations about the internal structure of an object without inserting a detector inside the human body [18]. This technique is based on the same principle as a SONAR. Its clinical applications are widespread: examination in obstetrics and gynecology, even in the early stage of the pregnancy, in guiding surgical implants or observation of the abdomen, infant brain, eyes and thyroid among others. Tissue at the microscopic level can also be characterised [19].

In many experimental studies, focused ultrasonic beams offer unique possibilities for creating lesions in animal tissues. High power ultrasound can be used to induce changes to a very localised area by the application of energy without damaging the surroundings. Another application in surgery involves the use of surgical instruments that are vibrated ultrasonically.

In dentistry ultrasound is used for a whole host of tasks including cleaning, polishing and drilling of tooth enamel. For example the removal of calcified plaques is achieved thanks to erosion due to cavitation. The projection of a spray on tooth containing air, water and carbonate sodium gives a cleaning/polishing effect.

If applications of ultrasound in daily life are numerous it is also widely developed in chemistry. This interest is so high that utilisation of ultrasound in chemistry constitutes an individual field of research.

1.4 Sonochemistry

The use of ultrasound to catalyse chemical reactions can be explained by the stirring and scrubbing effects that occur during cavitation. However, the enhancement of the homogeneous reaction rate is thought to be attributed to the presence of hot spots.

1.4.1 Streaming effect

Ultrasound promotes efficient mass transport [20]. Bubble motion, microstreaming and microjet formation are mechanisms attributed to be responsible for the increased mass transport rates observed [21-25]

Excited bubbles can be considered as secondary sound sources and their vibrations move neighbouring layers. As this type of streaming is confined into a restricted volume near the sound source, it is commonly termed microstreaming. Microstreaming was found to be more important when bubbles are located on a solid boundary and when the ultrasonic frequency drives bubbles at their resonant frequency[26].

Depending on the acoustic pressure amplitude and the viscosity of the sonicated fluid, four different characteristic regimes of microstreaming (Figure 1.9) were observed by Elder [27].

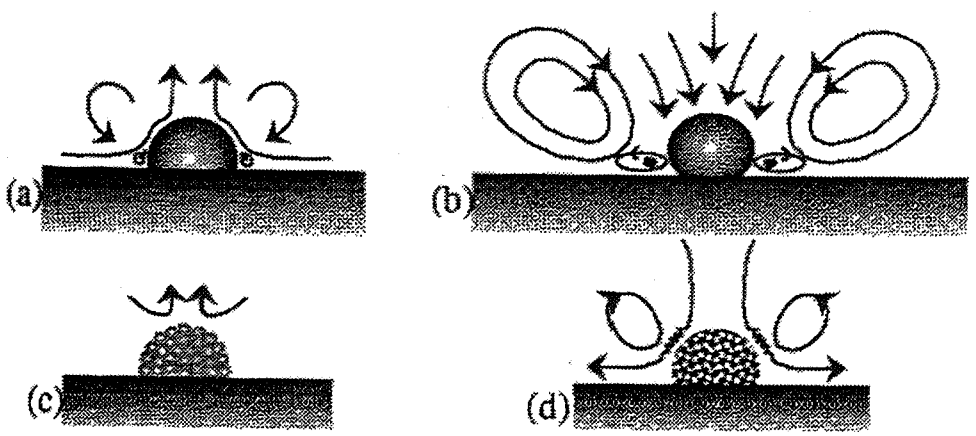

Figure 1.9: Several regimes of microstreaming (after Elder [27])

1.4.2 Scrubbing effect

The implosion of a bubble onto a solid surface provokes the erosion of this surface. This effect is shown in figure 1.10. The scrubbing effect of cavitation consist of removal, dissolution and under proper conditions destruction of surface contaminants. Hence surfaces of catalysts under ultrasonic irradiation are permanently reactivated.

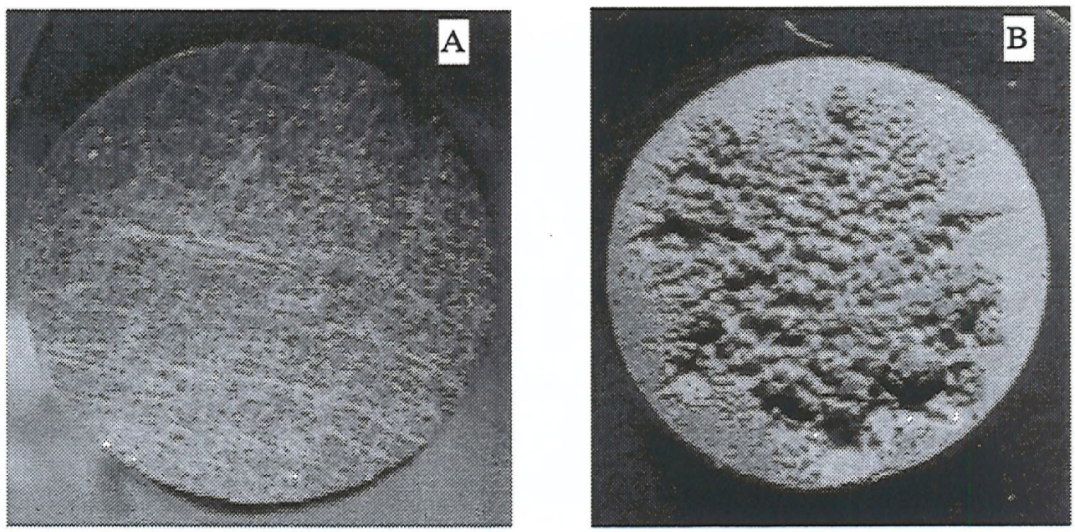

Figure 1.10: Pictures showing the scrubbing effect of ultrasounds after Birkin [28]. (A) shows an polished aluminium electrode, (B) shows the effect of ca. 30 min exposure to ultrasound.

This scrubbing effect is due to the following effects:

- A pressure pulse is emitted into the surrounding liquid when a bubble collapses. In a concentrated mass of bubbles, the shock wave induced by the collapse is transmitted to the surrounding bubbles and can provoke their implosion. Collapses become more and more energetic because the energy of each collapse is passed on to the following ones. Hence the combination of several bubble collapses is thought to provoke erosion.

- The second phenomenum causing the scrubbing effect is the formation of microjets during the asymmetric collapse of a cavity near a solid surface. In this case the damaged surface is small (one tenth the radius of the original cavity). As described in the numerical approach of Plesset and Chapman [29], asymmetry due to the presence of the solid plane provokes a reduction of the upward motion of the lower portion of

the bubble. Hence the bubble becomes elongated in the direction normal to the solid surface. As the bubble acquires kinetic energy, this energy is concentrated in the upper portion of the bubble. In the final stage of collapse, a jet is created, penetrating the bubble towards the boundary as a result of a higher collapse velocity of the upper bubble wall. This description has been confirmed by Lauterborn's [30] experiments on laser produced bubbles.

Both of the previous advantages of ultrasound are used in heterogeneous catalysis: there are several reports that the activity of a catalyst is improved by using ultrasound (compared to chemical methods) to prepare it [31]. Ultrasound can also be used to regenerate a catalyst. The intense stirring due to cavitation bubble collapse and acoustic streaming is also very useful in heterogeneous catalysis because the rate of production, the renewal of active sites and the desorption of products and poisons are enhanced.

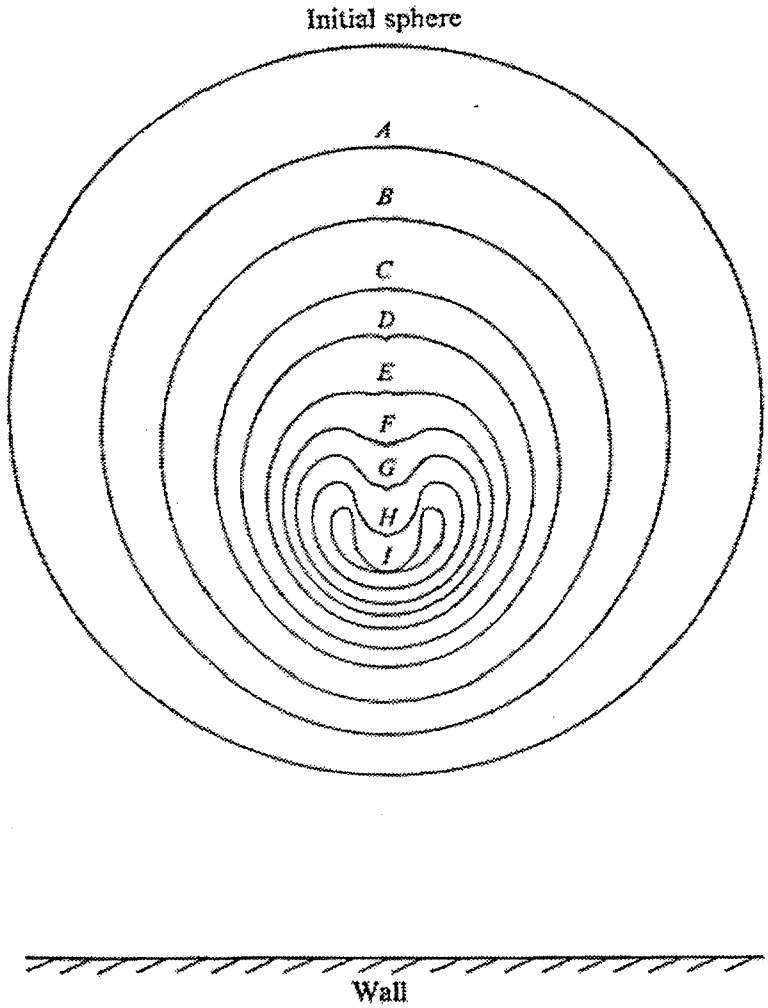

Figure 1.11: Asymmetric growth of a bubble due to the neighbourhood of a solid surface with creation of a microjet (after Plesset and Chapman [29])

Electrochemistry provides a good technique to study the enhancement of mass transport within a cavitating media [25]. This can be achieved by monitoring the current produced by the oxidation or reduction of an electroactive material at an electrode irradiated with ultrasound. In the case of a cylindrical reactor, where the emitting surface was located at the bottom of the cell, the mass transfer coefficient was found to change periodically along the direction of the sound wave [32]. This is in agreement with a standing wave pattern in the reactor. The mass transfer coefficient was also found to decrease from the emitter to the free surface of the liquid.

Indeed single cavitation events can be detected using microelectrodes [33]. This is because microelectrodes are small when compared to cavitation events. Moreover,

measurements of individual cavitation events as current-time transients can be made under mass transport limiting conditions.

1.4.3 Production of radicals

The process of cavitation is thought to produce extreme conditions of temperature (up to 3000 K) and pressure (up to 1000 bar) within the highly compressed gas phase of collapsing bubbles. These conditions provoke the dissociation of water into hydroxyl free radicals and hydrogen atoms:

$$H_2O \rightarrow OH^{\bullet} + H^{\bullet} \qquad \textit{Reaction 1}$$

The production of such radicals was first suggested by Weissler in 1959 [34]. However, their formation was only proved in 1982 by spin trapping [35]. In this spin trapping experiment a diamagnetic nitroso or nitrone compound was used to convert short-lived radicals into more stable species, the resultant nitroxyl radicals are ESR (electron spin resonance) observable. Estimation of hydroxyl radicals was firstly achieved by using the Fricke system [36]. Terephthalic acid is another radical scavenger used to monitor radical activity. This dosimeter provides the advantage that radical production is the only process involved. Rates of production of hydroxyl radicals are in the region of 10^{-6} mol dm^{-3} min^{-1} [37].

Radicals produced from reaction 1 may then recombine or react with other chemicals:

$$H^{\bullet} + OH^{\bullet} \rightarrow H_2O \qquad \textit{Reaction 2}$$

$$H^{\bullet} + H^{\bullet} \rightarrow H_2 \qquad \textit{Reaction 3}$$

$$OH^{\bullet} + OH^{\bullet} \rightarrow H_2O_2 \qquad \textit{Reaction 4}$$

$$OH^{\bullet} + OH^{\bullet} \rightarrow O^{\bullet} + H_2O \qquad \textit{Reaction 5}$$

$$2\,O^{\bullet} \rightarrow O_2 \qquad \textit{Reaction 6}$$

$$1/2\,O_2 + 2\,H^{\bullet} \rightarrow H_2O \qquad \textit{Reaction 7}$$

$$O_2 + H^{\bullet} \rightarrow HO_2^{\bullet} \qquad \textit{Reaction 8}$$

Production of $HO_2^{\bullet}$ was confirmed by conducting specific reactions involving this species. In the previous mechanism, generation of hydrogen peroxide can also be noticed. Hydrogen peroxide is also a well-known species in environmental chemistry[5].

Application of ultrasound to an aqueous solution is therefore thought to catalyse the degradation of impurities. This process involves three pathways: oxidation by hydroxyl radicals, pyrolytic decomposition and supercritical water oxidation. Volatile solutes such as CCl_4 will undergo direct pyrolisis reactions [38] within the gas phase of the collapsing bubbles or within the hot interfacial region. In the solvent layer surrounding the hot bubble, both combustion and free-radical reactions are possible. Pyrolisis in the interfacial region is predominant at high solute concentrations, while at low concentrations radical reactions become predominant.

Streaming, scrubbing and production of radicals are not the only effect of cavitation. The emission of light is another observable phenomenum.

1.5 Sonoluminescence

1.5.1 Phenomena

Sonoluminescence is the emission of light associated with transient cavitation. A picosecond flash of broadband light which extends well into the ultraviolet can be emitted during the collapse of a bubble. Flashes, for a single bubble, were found to be emitted very regularly. For some years, a certain form of stable cavitation was shown to sonoluminate too [39]. In fact, in such a case distinction between stable and transient cavitation is problematic. To observe light emission, cavitation should be energetic.

Like cavitation, the intensity of the light emitted depends on the frequency of the sound, the temperature, the hydrostatic pressure of the liquid and the nature of the solvent.

The nature of sonoluminescence is still controversial. Several theories have been proposed but no theory satisfies all scientists. Mechanisms proposed in the past fall into three classes: thermal, mechanochemical and electrical. There is also a quantum theory.

1.5.2 Theories

1.5.2a Thermal mechanisms

Heat is generated by the compression of gas and vapour during the collapse. However, this heat cannot be dissipated because thermal transport is slower than the bubble collapse. Hence, very high temperatures are attainable in the gas phase. In this hot-spot region free radicals and molecules in excited states are produced. Radiative recombination of these radicals and relaxation of the excited species generate the emission of light. This theory [40] is based on the high collapsing temperatures, on the detection of radicals and on sonoluminescence spectra. Sonoluminescence spectra of hydrocarbons show vibrationally resolved bands that can be attributed to emission from the excited state of diatomic molecules.

1.5.2b Electrical mechanisms

These theories assert that charging of gas-filled bubbles in solution occurs, producing an electrical microdischarge that is the source of light. Margulis [41] considers a bubble at larger than resonant size that has been made from the coalescence of smaller bubbles. A process observed with such a bubble is the formation of a smaller bubble off the side of the large one. An electrical double layer is formed between the small and the large bubble. As the smaller bubble is removed, the charge from a large area of the large bubble is assumed to concentrate on a small area of the small bubble. The rate of formation of the bubble is assumed to be faster than the rate of charge diffusion along its surface, so that a large negative charge develops on the smaller

bubble. A discharge through the smaller bubble occurs after separation to equalise the charges.

1.5.2c Mechanochemical mechanisms

The passage of a shock wave through a gas is accompanied by a burst of visible radiation. The emission of such shock wave is possible when the bubble wall speed exceeds the speeds of sound in both gas and liquid [42].

For A. Prosperetti [43], the emission of light is associated with the fracture of the sonicated liquid. In his words "the sonoluminescence lower threshold coincides with the pressure amplitude at which the jet developing during the collapse phase impacts (with sufficient energy) the opposite side of the bubble. The upper threshold is due to the total disruption of the integrity of the bubble when the impact becomes too violent."

1.5.2d Sonoluminescence as quantum vacuum radiation

Sonoluminescence is explained in terms of quantum vacuum radiation by moving interfaces between media of different polarisability [44, 45]. This assertion is confirmed by the fact that no photons in the UV are emmited. Moreover, expected pulse lengths are of the same order as those found experimmentally.

1.5.3 Sonochemiluminescence

Alkaline solutions of luminol have been known to enhance light emission when exposed to ultrasound [46]. Compared to sonoluminescence of an aerated aqueous solution, the intensity of the emmitted light is increased. Hydroxyl radicals produced by transient cavitation are thought to be involved but the exact mechanism of this reaction is still unknown [47].

1.6 Theoretical prevision of pressure field

As shown in 1.2.1b the acoustic pressure field determines the type of cavitation. Hence, study of the pressure field within a chemical reactor gives an indication of the chemically active regions. The general wave equation of pressure [48] is given by equation (1).

$$\nabla^2 P = \frac{1}{c^2}\ddot{P} \tag{13}$$

where c is the sound speed.

In the case of a cylindrical cell and using the appropriate boundary conditions (pressure nodes at the interfaces), equation (13) can be solved and gives equation (14).

$$P(r,z,t) = i\rho\sum_{n=0}^{\infty}\omega A_{n,z} J_0\left[j_{0,n}\frac{r}{a}\right]e^{i(\omega t - k_z z)} \tag{14}$$

where ρ, $A_{n,z}$, n, a, $j_{0,n}$, and ω represent the density of the medium, the amplitude of the particular mode, integer denoting the mode assignment, the radius of the cell, the value of the Bēssel function and the frequency of the sound wave respectively.

The net wave vector '*k*' can be determined from the pythagorean sum of the component terms (k_z and k_r) under these conditions equation (15)

$$k = \sqrt{k_z^2 + k_r^2} = \frac{\omega}{c} = \frac{2\pi}{\lambda} \tag{15}$$

$$k_r = \frac{j_{0,n}}{a}$$

where $j_{0,n}$ represents the value of the Bessel function at the boundary conditions.

In order to solve equation (15), the boundary conditions at the interface with the liquid , two cases have to be considered:

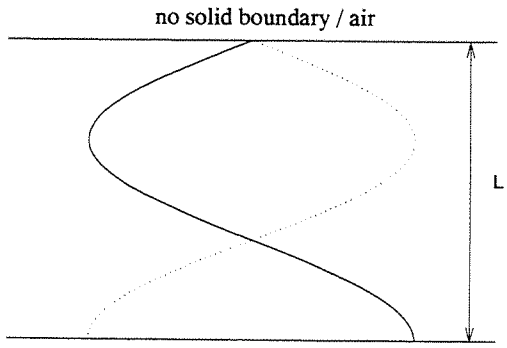

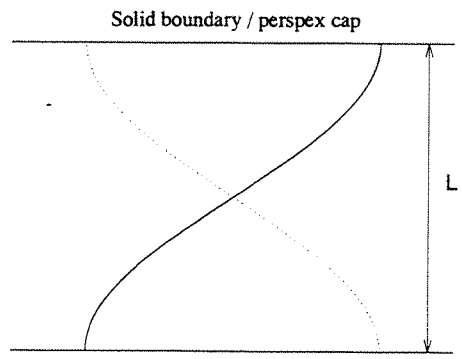

In a standing wave pattern the height of liquid should respect the following condition:

$$L = \frac{q\pi}{4},$$

where q = 2n+1 and n = 0, 1, 2 ...

$$L = \frac{q'\pi}{4},$$

where q' = 1, 2, 3 ...

Therefore the axial component of the wave reactor is equal to:

$$k_z = \frac{2q\pi}{4L} = \frac{q\pi}{2L}$$

$$k_z = \frac{2q'\pi}{2L} = \frac{q'\pi}{L}$$

By replacing the axial and radial component of the wave vector by their value in equation (15) the sound frequencies which sustain a standing wave field can be deduced:

$$f = \frac{c}{2\pi}\sqrt{\left(\left(\frac{j_{0,n}}{a}\right)^2 + \left(\frac{q\pi}{2L}\right)^2\right)} \qquad (16)$$

$$f = \frac{c}{2\pi}\sqrt{\left(\left(\frac{j_{0,n}}{a}\right)^2 + \left(\frac{q'\pi}{L}\right)^2\right)} \qquad (17)$$

In such conditions, pressure maxima are expected to be in a ring pattern in the radial direction and along the axis bands at equal distance from each other [49]. The distances between rings or between bands are strongly dependent on the applied frequency waves. If the frequency is increased, the pressure maxima of the resonant mode will become closer.

In this thesis pressure within the cell, which determines the nature of cavitation, will be studied spatially and as a function of frequency. Influence of frequency on physical properties of the transducer and sound output will also be investigated. These studies will later on lead to a comparison with two obervable consequences of cavitation, luminescence and sonochemistry of sonicated solutions.

References

[1] G. Ruppert, R. Bauer, G. Heisler, *Journal of photochemistry and photobiology A 73* (1993) 75.

[2] M. H. Al-Malack, G. K. Anderson, *Water research 31* (1997) 3064.

[3] J. Cho, G. Amy, J. Pellegrino, *Water research 33* (1999) 2517.

[4] A. J. Poole, R.Cord-Ruwisch, F. W. Jones, *Water research 33* (1999) 1981.

[5] A. Alvarez-Gallegos, D. Pletcher, *Electochimica Acta 44* (1999) 2483.

[6] J. Thornycroft, S. W. Barnaby, *Instit. Civil. Eng. 122* (1895) 51.

[7] Young, *Cavitation*, Mc Graw-Hill 1989, p. 40.

[8] K. S. Suslick, G. J.W., P. F. Schubert, H. H. Wang, *J. Phys. Chem. 87* (1983) 2299.

[9] J. P. Lorimer, in T. J. Mason (Ed.): *Sonochemistry: the uses of ultrasound in chemistry* 1990, p. 9.

[10] G. Kurtze, *Nachr. Akad. Wiss. Goettingen II A* (1958) .

[11] S. Silva-Martinez, *Department of chemistry*, University of Southampton 1997.

[12] J. P. Perkins, in T. J. Mason (Ed.): *Sonochemistry: the uses of ultrasound in chemistry*, The royal society of chemistry 1990.

[13] A. P. Cracknell, *Ultrasonics*, Wykeham Publications 1980, p. 74.

[14] D. Hibberd, A. Holmes, M. Garrood, A. Fillery-Travis, M. Robins, R. Challis, *Journal of colloid and interface science 193* (1997) 77.

[15] A. K. Gurvich, in N. P. Borogoditskii (Ed.): *The physics and applications of ultrasonics* 1962, p. 119.

[16] T. J. Mason, L. Paniwnyk, J. P. Lorimer, *Ultrasonics sonochemistry 3* (1996) 253.

[17] P. K. Chendke, H. S. Fogler, *Ultrasonics* (1975) 31.

[18] C. S. Gartside, M. M. Robins, in T. J. Mason (Ed.): *Sonochemistry: the uses of ultrasound in chemistry* 1990, p. 27.

[19] *Ultrasound: its applications in medicine and biology*, Elsevier 1978.

[20] P. R. Birkin, S. Silva-Martinez, *Journal of Electroanalytical Chemistry 416* (1996) 127.

[21] S. A. Perusich, R. C. Alkire, *J. Electrochem. Soc. 138* (1991) 700.

[22] R. G. Compton, J. C. Eklund, S. D. Page, *J. Phys. Chem. 99* (1995) 4211.

[23] J. Klima, C. Bernard, C. Degrand, *J. Electroanal. Chem. 367* (1994) 297.

[24] F. Faid, F. Contamine, A. M. Wilhelm, H. Delmas, *Ultrasonics Sonochemistry 5* (1998) 119.

[25] J. Reisse, H. Francois, J. Vandercammen, O. Fabre, A. K.-d. Mesmaeker, C. Maerschalk, J.-L. Delplancke, *Electrochimica acta 39* (1994) 37.

[26] J. Kolb, *J. Acoust. Soc. Am. 28* (1956) 1237.

[27] S. A. Elder, *J. Acoust. Soc. Am. 31* (1958) 54.

[28] P. R. Birkin, R. O'Connor, C. Rapple, S. S. Martinez, *J. Chem. Soc., Faraday Trans. 94* (1998) 3365.

[29] M. S. Plesset, R. B. Chapman, *J. Fluid Mech. 47* (1971) 283.

[30] W. Lauternborn, H. Bolle, *J. Fluid Mech. 72* (1975) 391.

[31] J. Lindley, in T. J. Mason (Ed.): *Sonochemistry: the uses of ultrasound in chemistry* 1990, p. 102.

[32] F. Trabelsi, H. Ait-Lyazidi, B. Ratsimba, A. M. Willhelm, H. Delmas, P.-L. Fabre, J. Berlan, *Ultrasonics sonochemistry 3* (1996) .

[33] P. R. Birkin, S. Silva-Martinez, *Ultrasonics Sonochemistry 4* (1997) 121.

[34] A. Weissler, *J. Am. Chem. Soc. 81* (1959) 1077.

[35] K. Makino, M. M. Mossoba, P. Riesz, *J. Am. Chem. Soc. 104* (1982) 3537.

[36] A. K. Jana, S. N. Chatterjee, *Ultrasonics sonochemistry 2* (1995) 87.

[37] G. J. Price, E. J. Lenz, *Ultrasonics 31* (1993) 451.

[38] M. R. Hoffmann, I. Hua, R. Hoechemer, *Ultrasonics sonochemistry 3* (1996) 163.

[39] D. F. Gaitan, L. A. Crum, C. C. Church, R. A. Roy, *J. Acoust. Soc. Am. 91* (1992) 3166.

[40] K. S. Suslick, S. J. Doktycz, E. B. Flint, *Ultrasonics 28* (1990) 280.

[41] M. A. Margulis, *Ultrasonics 23* (1985) 157.

[42] P. W. Vaughan, S. Leeman, *Acustica 59* (1986) 279.

[43] A. Prosperetti, *J. Acoust. Soc. Am. 101* (1997) 2003.

[44] C. Eberlein, *Physical review A 53* (1996) 2772.

[45] C. Eberlein, *Physical review letters 76* (1996) 3842.

[46] A. Henglein, D. Herburger, M. Gutierrez, *J. Phys. Chem. 96* (1992) 1126.

[47] B. P. Wilson, *Department of Materials Engineering*, University of Wales, Swansea 1998.

[48] T. G. Leighton, *The acoustic bubble*, Academic Press 1994, p. 101.

[49] P. R. Birkin, T. G. Leighton, C. L. Delaplace, T. Bayliss, M. D. Simpson, *awaiting for publication* (1999) .

2. Experimental

2.1 Apparatus

2.1.1 Generation of ultrasound

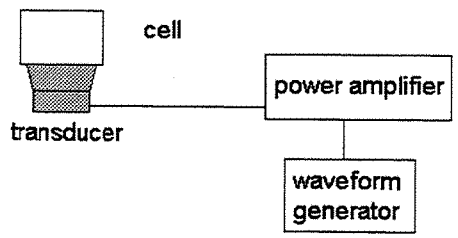

Figure 2.1: Description of the set-up used to generate ultrasonic waves

Experiments were carried out in two types of cells (cf. table1). These cells were fixed to a sandwich piezoelectric transducer with Quick set epoxy resin. Transducers were all supplied by Morgan Matroc Limited. As seen in figure 2.2, transducers are made of two piezo-ceramic rings sandwiched between two metal layers. When an electric field is applied to such piezoelectric materials, the crystalline structure changes shape, producing dimensional changes in the material.

	100 ml cell	**scale-up experiments**
type of cell	jacketed glass cell	perspex
resonant frequency of the transducer	25 kHz	33 kHz

Table 1: Resonant frequency of the transducer for each cell

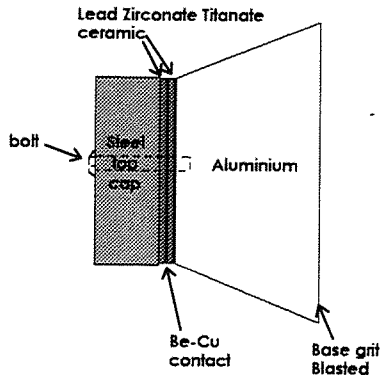

Figure 2.2: Transducers are made of two piezo-ceramic rings sandwiched between two metal layers

In order to produce cavitation, the transducer was driven by a Thurbly Thandar instrument's generator (TG 1010) via a power amplifier (Brüel & Kjær, type 2713). This generator allows the frequency of the ultrasound signal to be easily changed over a range of 20 kHz to 160 kHz. For all the experiments, the power amplifier was adjusted to obtain V_{RMS} = 90V (and V_{RMS} = 80V for scale-up experiments).

2.1.2 Pressure measurements

Pressure in the cell was measured using a Brüel & Kjær 8103 hydrophone (figure 2.3) connected to a Brüel & Kjær 2635 charge amplifier. Such measurements were again achieved using the piezoelectric effect. The hydrophone was made of piezoelectric ceramics, which act as sensors to convert the mechanical stress into an electric signal. In relation to the wavelength of sound used in this study, the size of the sensitive part of the hydrophone is relatively small, therefore measurements are almost omnidirectional [1]. The electric output signal was measured on an Gould 465 oscilloscope. The set-up is shown on picture 2.7.

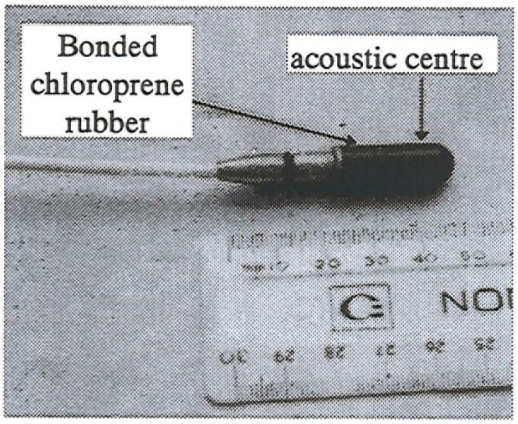

Figure 2.3: The figure shows Brüel & Kjær 8103 hydrophone suitable for measurements from 50 Hz to 200 kHz.

Audible sound (from 20 Hz to 20 kHz) above the cell was also measured using a Brüel & Kjær 4191 microphone connected to an Brüel & Kjær 2609 amplifier. The microphone was placed 3.5 cm away from the surface of the liquid.

2.1.3 Photoncounter

As shown on figure 2.4, measurements of light emission were achieved by employing a EG Σ G photon counting module (module SPCM-200-PQ) connected to a PC. In such a device the emission of photons per channel (or per unit of time, this unit of time was chosen in the software) was recorded during the irradiation of the solution.

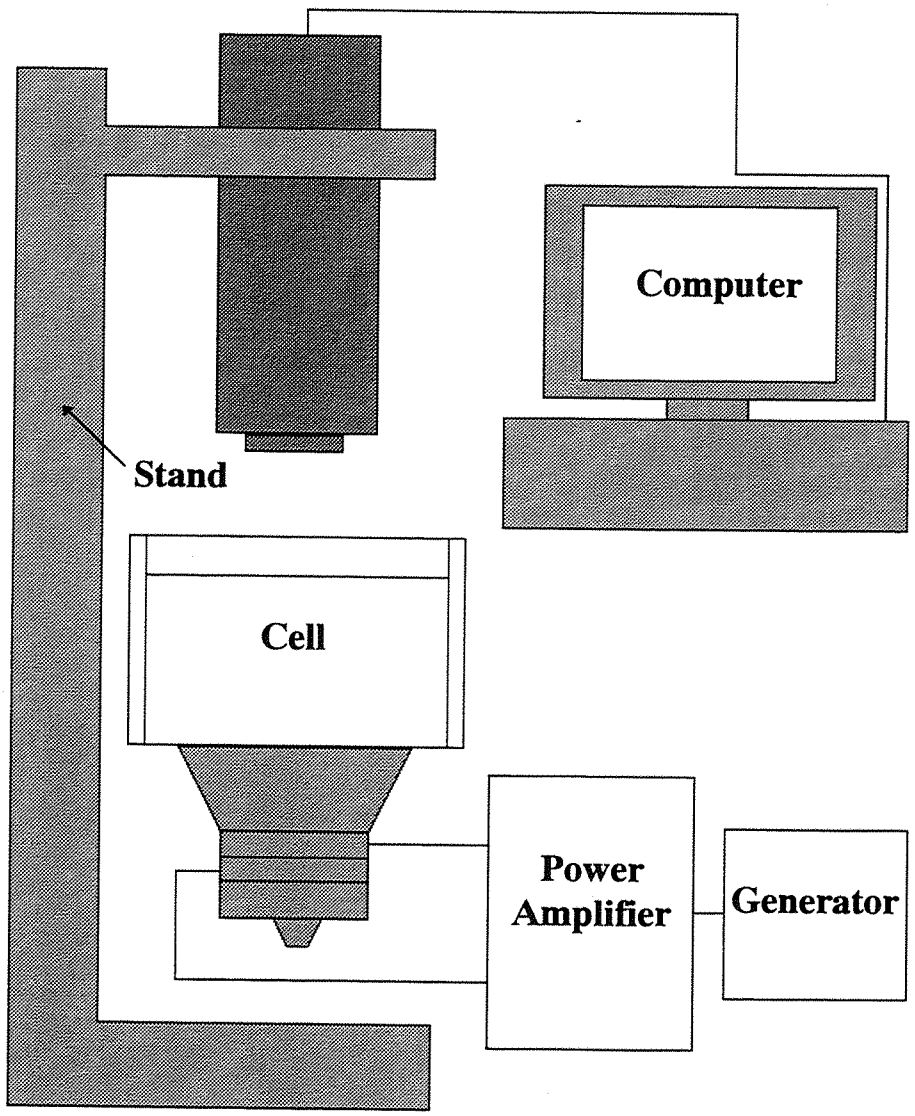

Figure 2.4: The figure shows the set-up designed to record the light emission from a sonicated solution

2.1.4 Low light camera

Pictures from the light pattern emitted from an alkaline solution of luminol were also recorded. The set-up is described on picture 2.5.

Video footage showing the active zones within the cell were taken using an image intensified CDD camera (Photonic Science). The camera was fitted with a Fuji 25-mm lens. Pictures were recorded on a common video recorder. Pictures from these films were later extracted.

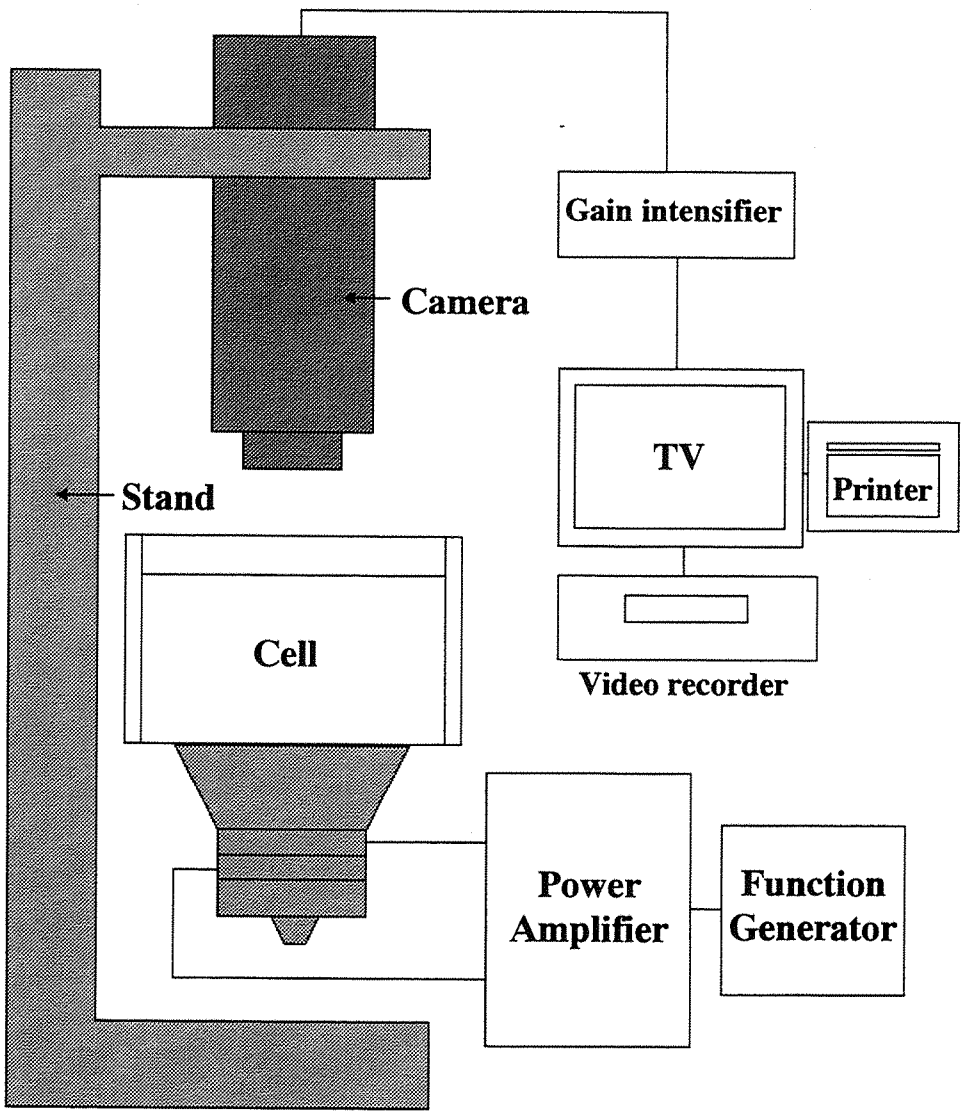

Figure 2.5: Shematic diagrm of the experimental set-up designed to record the light pattern emitted from a sonicated solution

2.1.5 Spectrophotometer

A Hewlett Packard 8452A diode array spectrophotometer connected to a PC was used to measure changes in solution absorbance at a chosen wavelength.

2.1.6 Electrochemical equipment

All experiments were performed in a Faraday cage in order to reduce the electrical noise. An Oxford electrodes bipotensiostat connected to a Hi-Tek 101 function

generator was employed. The electrochemical signal was recorded by a PC via an Analogic Digital Computer card (Talisman Electronics, Computer Boards CIO-DASO8-PGL).

2.2 Cells

A perspex cell was used in scale-up experiments, all other experiments were carried out in a jacketed glass cell. Properties and description of cells are listed in the following table:

	glass cell	perspex cell
description	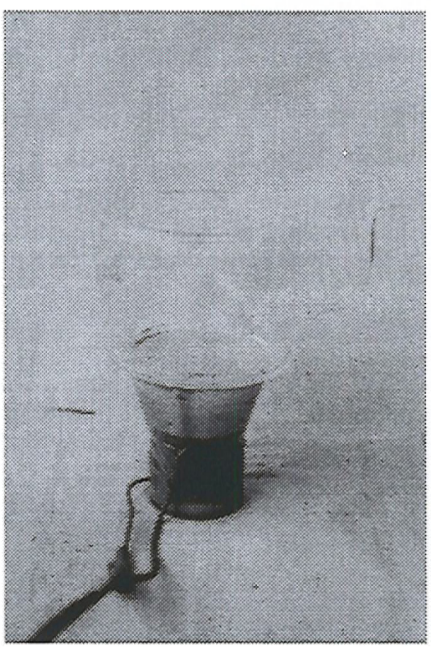	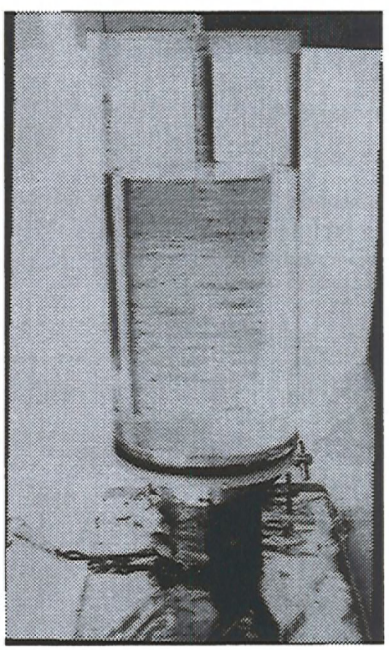
capacity	100 ml	up to 1 litre
inner radius (mm)	28.6	46
thermal regulation	yes, 25°C	no

Table 2: Description and properties of cells used for early experiments and in scale-up experiments.

2.3 Chemicals

Chemicals	Purity/%	Supplier
3-aminophthalhydrazide(luminol)	97	Aldrich
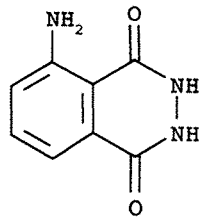		
Hexaamine ruthenium (III) chloride ($[Ru(NH_3)_6]Cl_3$)	99	Strem Chemicals
Hydrochloric acid	35.4	Fisons
Hydrogen peroxide	30	Sigma
Meldola blue		BDH
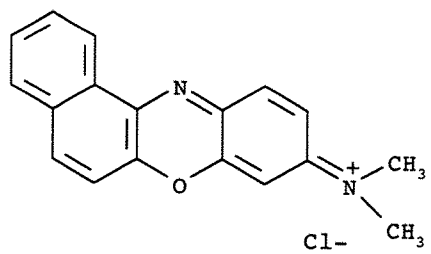		
Potassium chloride	99.9	BDH
Potassium iodide	99	HOGG
Sodium carbonate anhydrous	99.9	BDH
Sodium chloride	99.9	BDH

Aqueous solutions were prepared with water purified from a Whatman RO 50 reverse osmosis process followed by a Whatman "Stillplus" water purification system. For the experiments using the perspex cell, another purification unit was used, Elect (USF), the first step of the purification process was the same, reverse osmosis, then water was passed through an ADEPT electrical deionisation module and UV lamp (photo-oxidation). Both water systems produce organic free, low conductivity, water (<15MΩ cm^{-1}).

2.4 Experimental procedure

2.4.1 Impedance measurement

The application of an alternating current signal, in presence of a DC ramp, allowed measurement of the electrical resistance and the reactance of the transducer.

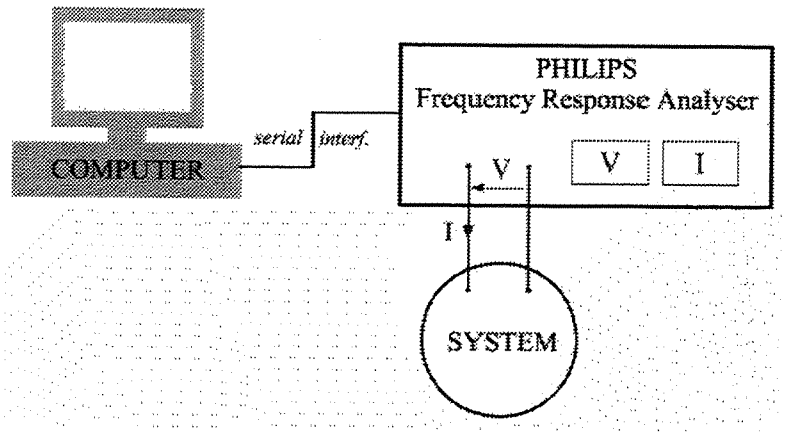

Figure 2.6: Set-up used to measure the impedance of either the transducer alone or the cell cointaining 100 ml of solution and attached to the cell.

2.4.2 Pressure measurement

Figure 2.7 describes the set-up used to determine the pressure field within the cell.

The pressure was measured for different positions of the hydrophone as a function of frequency. Variations of the pressure within the cell were also measured during the irradiation of the solution at 122 kHz. In such experiments the hydrophone was moved in radial directions and along the axis of the cell by the use of a micrometer-positioner. The solution contained 10 mmol dm^{-3} HCl and 0.1 mol dm^{-3} NaCl. To avoid modification of the irradiation conditions the height of solution in the cell was kept constant. To achieve this the sum of the volumes of the hydrophone immersed part and the solution within the cell was always equal to 100 ml.

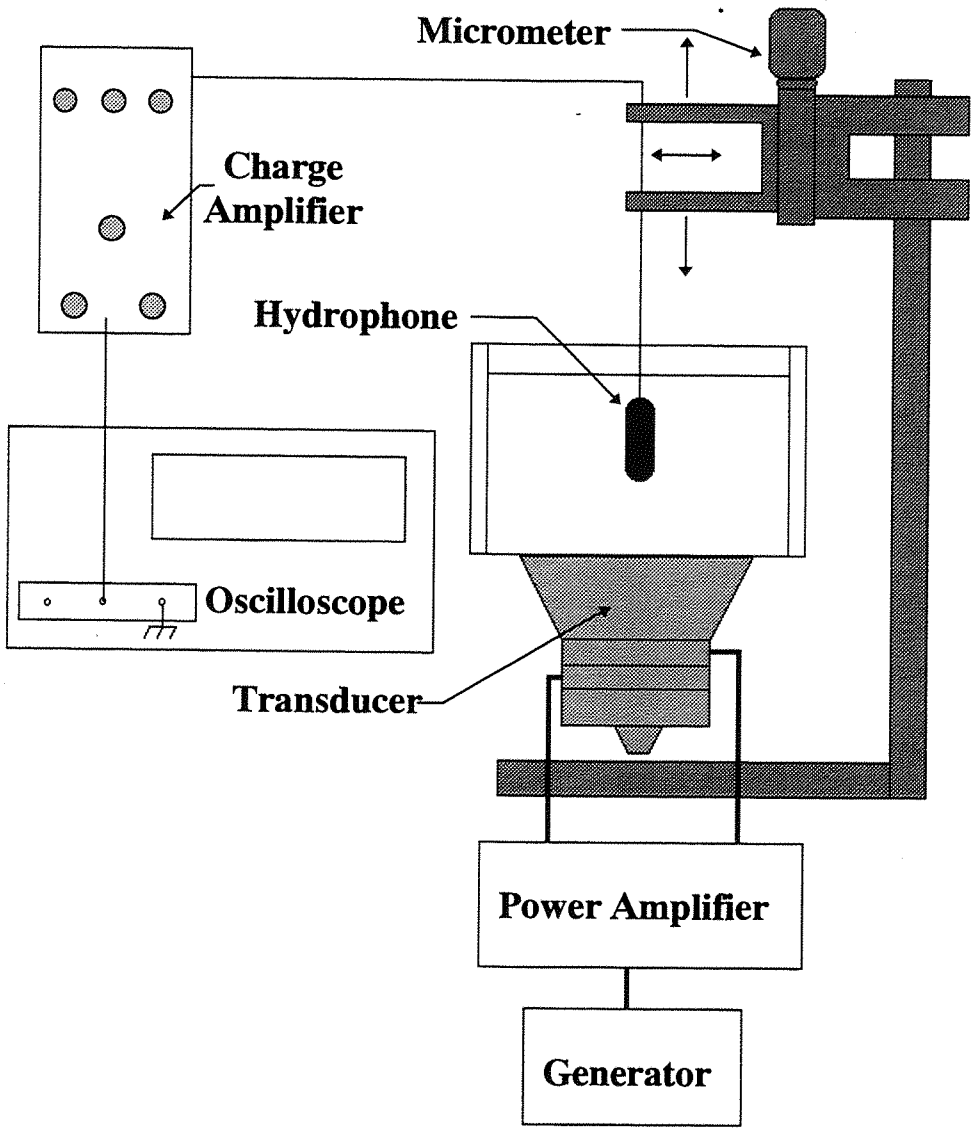

Figure 2.7: The figure shows the set-up to measure the pressure field within the cell

In order to avoid distortion of the acoustic signal recorded, small bubbles attached to the hydrophone were removed each time the frequency was changed and a new measurement was made.

It was noted that for certain frequencies the acoustic signal varied strongly with time, in both shape (figure 2.8) and amplitude (figure 2.9). In such cases an average of the highest observable amplitude on several records was calculated to give an approximation of the pressure amplitude. This value was then used to describe pressure as a function of frequency (cf. paragraph 3.4).

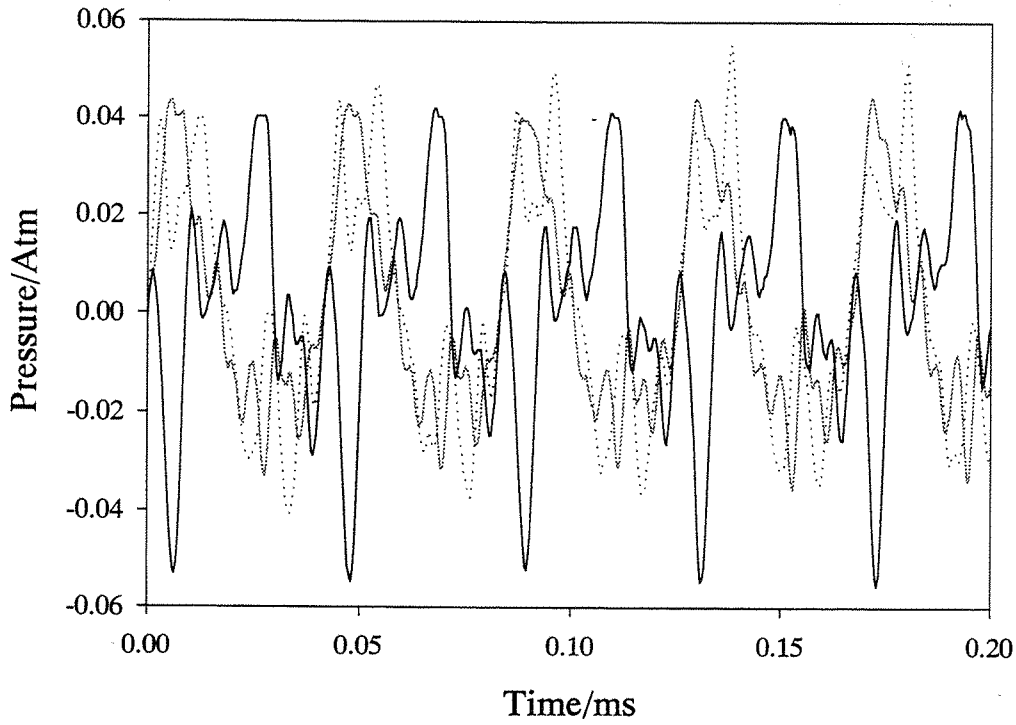

Figure 2.8: The figure shows several records of pressure measurement as a function of time. All these plot were recorded during the irradiation of a 100 ml electrolyte solution at 24 kHz. For all these records the hydrophone was placed at the same position within the cell.

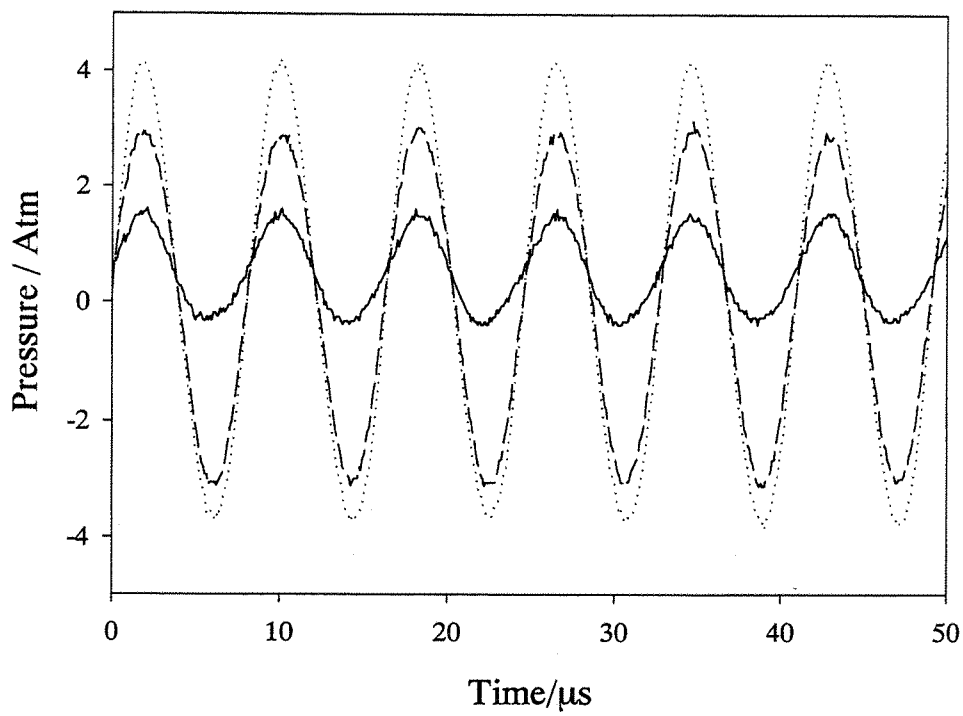

Figure 2.9: The figure shows the variation of pressure amplitude for a same position of the hydrophone. These records were achieved during the irradiation at 122 kHz of a 100 ml electrolyte solution.

2.4.3 Output power measurement

As seen in figure 2.10, a resistor was put in series with the cell. The voltage amplitude of the resistor and of the power amplifier were measured, the phase angle between both was also calculated. These measurements were achieved using a 200 MHz DSO 465 Gould oscilloscope.

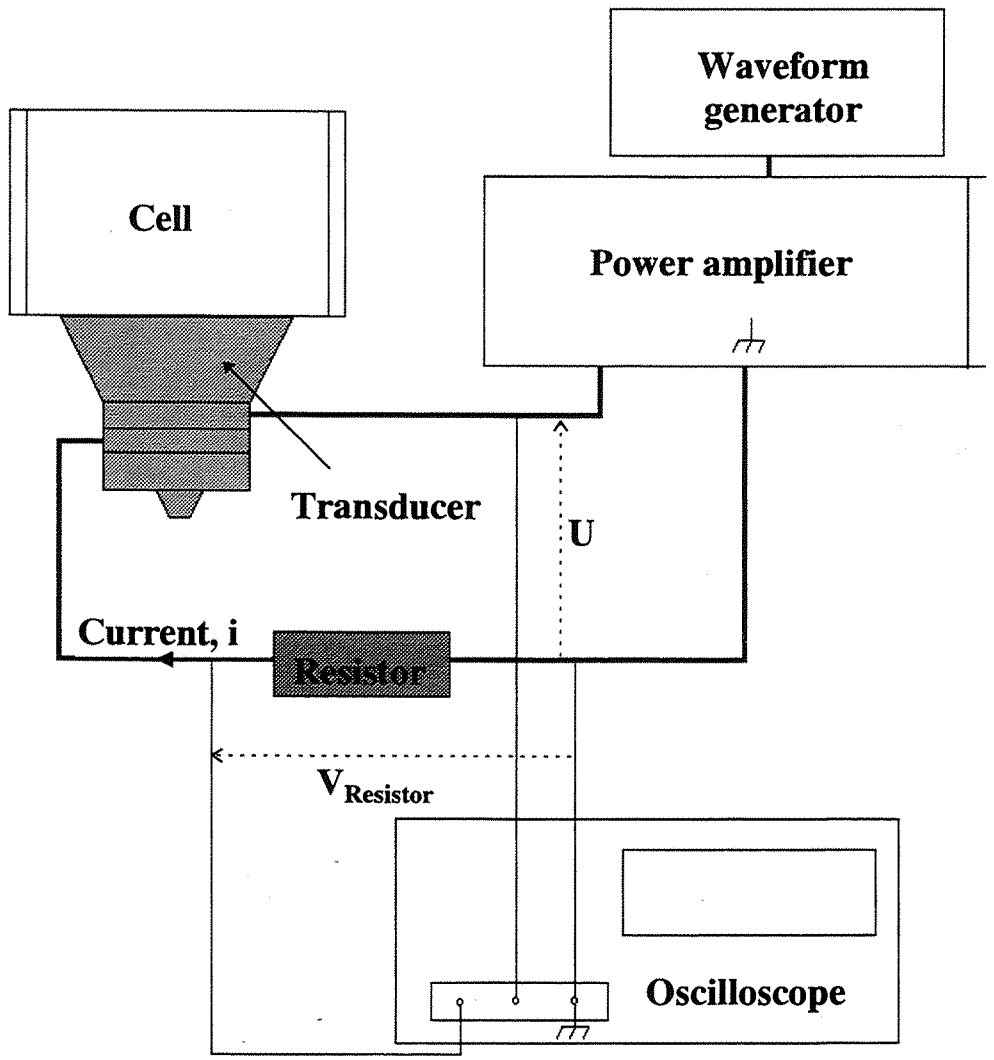

Figure 2.10: Figure showing the experimental set-up designed to measure the output power from the power amplifier.

The active output power from the generator was calculated using the following equation:

$$W = U \times I \times \cos\phi$$

with:

$$I = \frac{V_{resistor}}{R}$$

where U, I, $V_{resistor}$, R, ϕ represent the voltage amplitude of the power amplifier, the current crossing the resistor, the voltage amplitude of the resistor, resistance and the phase shift between the current and the power amplifier voltage. The phase shift is defined by:

$$\phi = \frac{t}{T} \times 2\pi$$

where t is the time shift between the current and the voltage and T is the period of the signal (see figure 2.11).

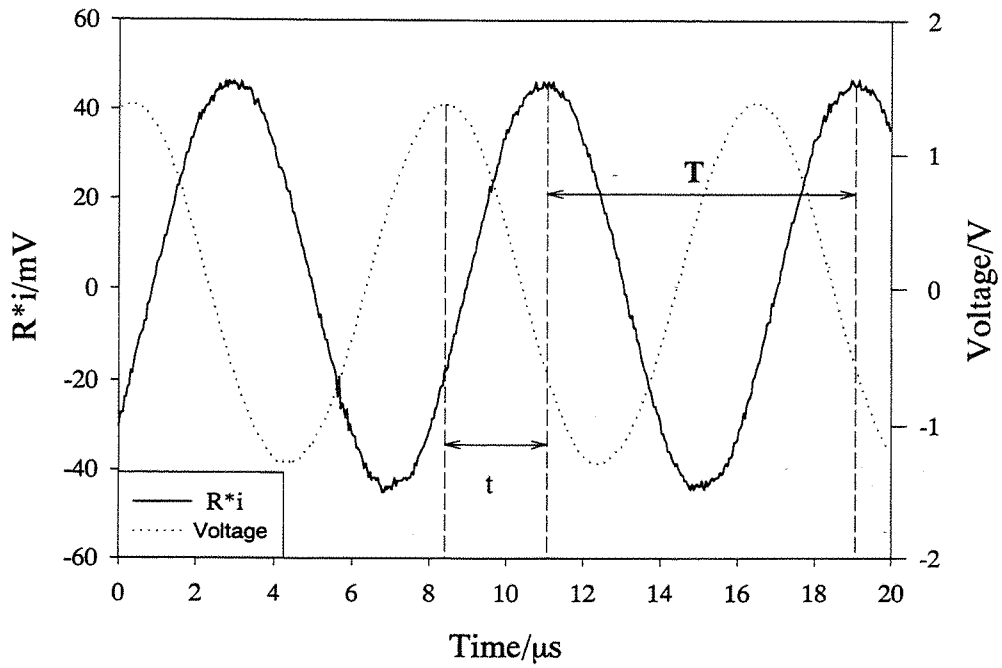

Figure 2.11: Measurements of the output current (solid line) and voltage (dotted line) from the generator during the irradiation at 124 kHz.

2.4.4 Sonoluminescence experiment

All experiments were carried in a dark room, the cell and the photoncounter were also put into a carton box covered with dark cotton sheets in order to reduce the light noise. With such a set-up, small variations of the photoncounter position relative to the cell were not found to significantly affect measurements.

Two types of experiments were carried out. Emission of light from an electrolyte solution was first measured, in the second case production of light was enhanced by adding luminol (a compound reacting with hydroxyl radicals to give light emission). Solutions containing 1.0 or 1.2 mmol dm^{-3} luminol and 50 mmol dm^{-3} Na_2CO_3 were employed.

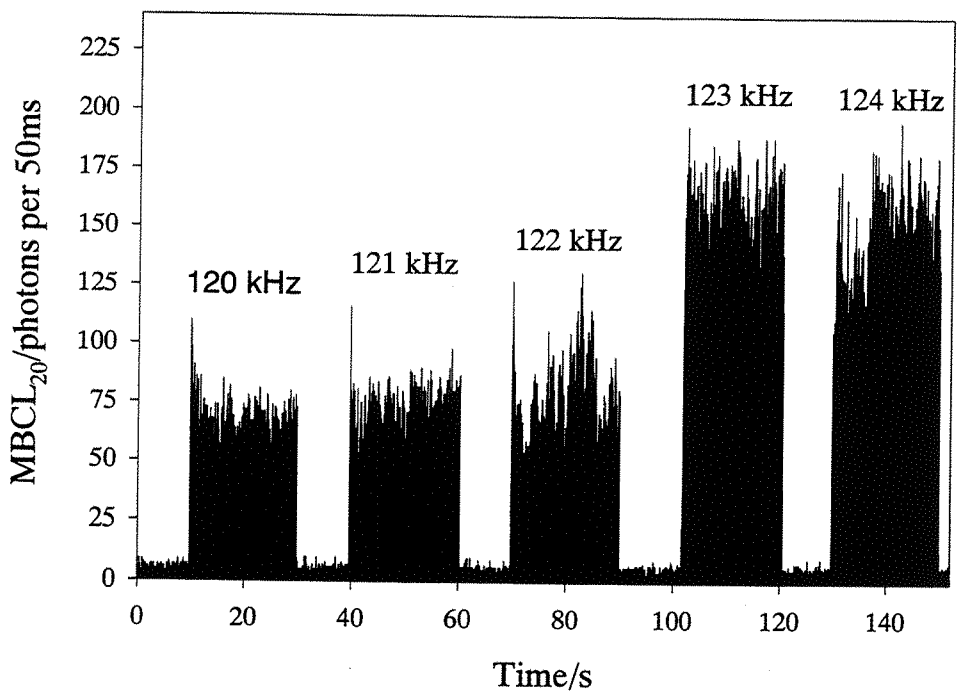

Figure 2.12: Photoncount of the luminescence from a sonicated solution of 0.1 mol dm^{-3} NaCl and 10 mmol dm^{-3} HCl. The solution is irradiated during 20 seconds and then no more irradiated during 10 seconds. During this silent period the frequency is increased by 1 kHz. The photoncount is achieved per 50 ms time lapse.

For a given solution, photoncounting was performed during 20 seconds of irradiation followed by 10 seconds when the solution was not irradiated. During this

silent period the driving frequency was increased by 1 kHz. Irradiation at this new frequency and measurement of the light emission were performed during 20 seconds and so on (see in figure 2.12). During the twenty seconds of irradiation, multiple photoncounts were achieved (in fact -20s divided by the chosen unit of time- times. An average of these measurements was then used as the final photoncount measurement.

2.4.5 Degradation of Meldola blue

Solutions of 0.1 mmol dm^{-3} Meldola blue in electrolyte (0.1 mol dm^{-3} NaCl and 10 mmol dm^{-3} HCl) were irradiated at different frequencies. The choice of Meldola blue as an organic impurity was justified by the following aspects: Meldola blue is cheap, it is strongly coloured (even at very low concentration) and it loses its colour in the first step of its degradation (destruction of the conjugaison).

For a given cell and at a given frequency, two 1 ml samples of solution were taken and each was added to 4 ml of distilled water. These samples were then analysed by a Hewlett Packard 8452A diode array spectrophotometer at l = 570 nm in a plastic cuvette. For a set of experiments (i.e. at a given frequency), all spectrophotometric measurements were achieved in the same cuvette.

2.4.6 Oxidation of iodide

The set-up shown on figure 2.14 was used to follow the concentration of iodine during irradiation.

100 ml of iodide solution (100 mmol dm^{-3}) was degassed with argon during 10 minutes and then irradiated with ultrasound at a given frequency. Tubing and a flow cell were filled with degassed solution before to the start. In this way, the volume of solution in the cell was always equal to 100 ml.

The irradiated solution was driven trough the flow cell as shown on figure 2.13 where triiodide concentration was measured by chronoamperometry using a platinum

electrode (0.5 mm) or a 10 μm diameter Pt microelectrode as a working electrode. The potential applied to the electrode was set to 0.2 V versus SCE. The calibration of the peristaltic pump (figure 2.15) and the determination of the mass transfer coefficient (figure 2.16) were made with a degassed 5 mmol dm^{-3} hexaamine ruthenium (III) chloride, $[Ru(NH_3)_6]Cl_3$ and 0.1 mol dm^{-3} KCl solution. For a given flow rate, the steady state current was measured (figure 2) and from this value the mass transfer coefficient was calculated through equation (18).

$$k_m = \frac{i_{ss}}{n \times F \times S \times C} \qquad (18)$$

where i_{ss}, n, F, k_m, S, C represent the steady state current, the number of exchanged electrons, the Faraday constant, mass transfer coefficient, the surface of the electrode and the concentration of the ruthenium complex respectively.

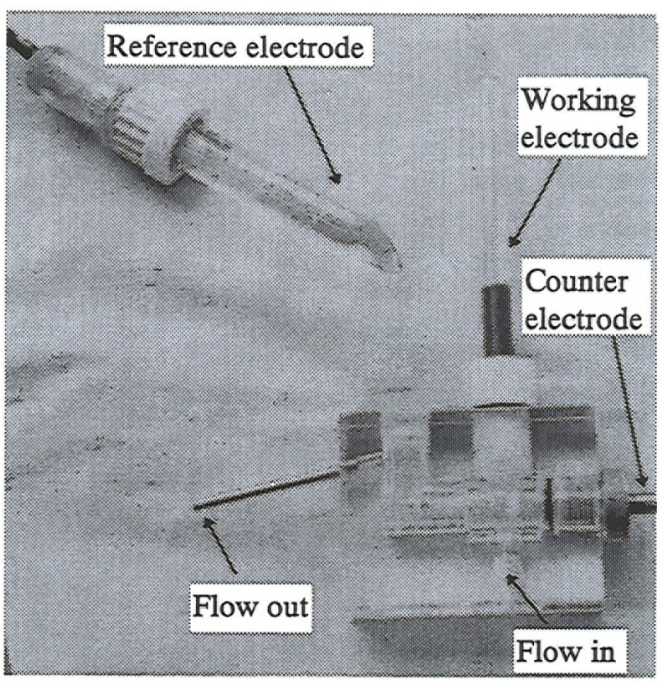

Figure 2.13: The figure shows the flow cell and electrodes used to determine the concentration of triiodide

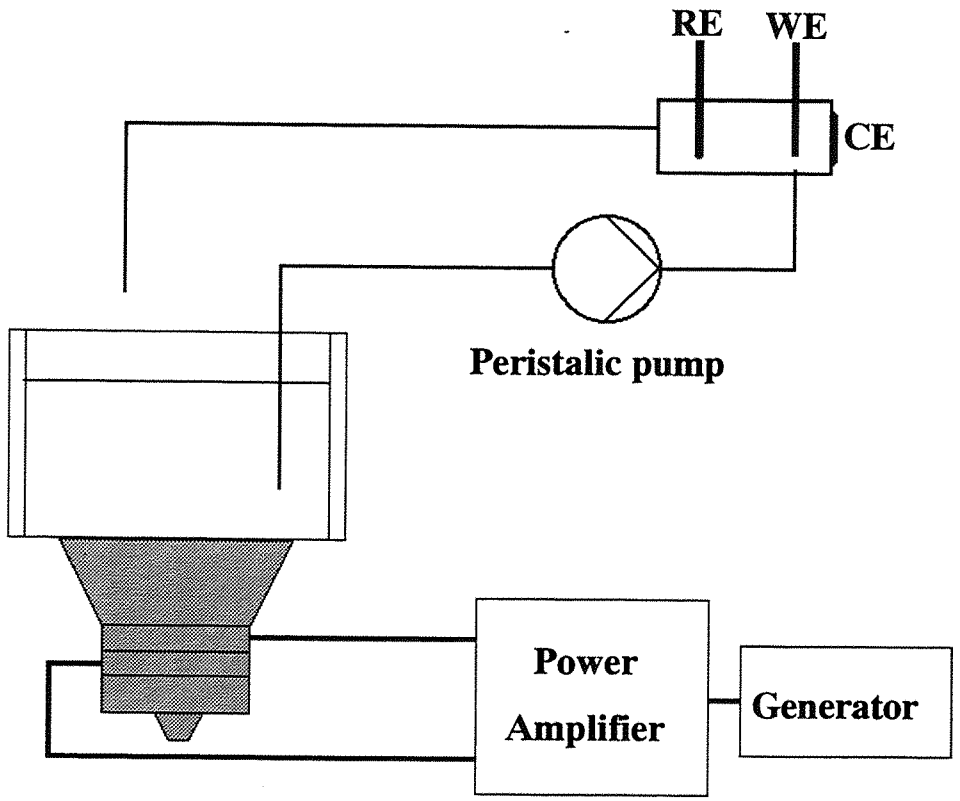

Figure 2.14: The figure shows the experimental set-up used to oxidise iodide into triiodide and to detect by electrochemistry the concentration of triiodide formed.

Diffusion coefficients for triiodide ($D = 9 \times 10^{-6}$ cm^2 s^{-1}) and for ruthenium are very similar [2], therefore the mass transfer coefficient of triiodide will be assumed to be equal in further calculations.

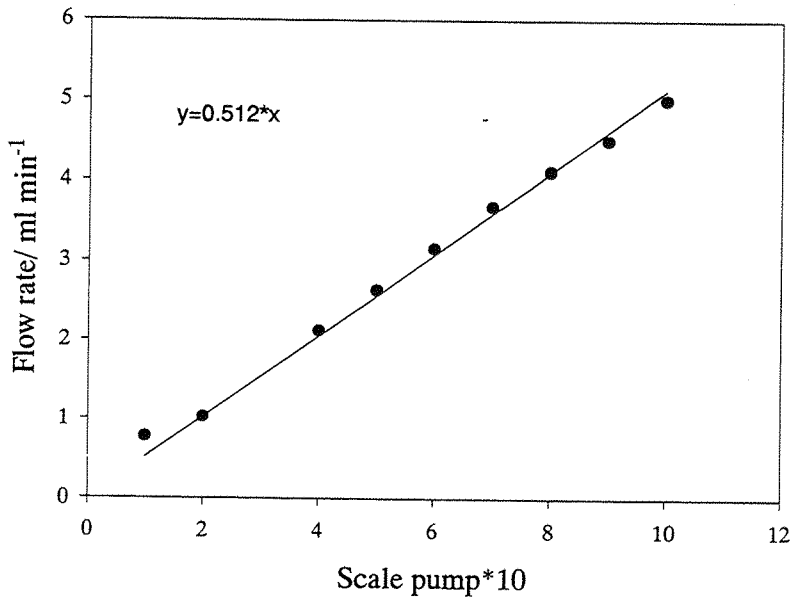

Figure 2.15: Flow calibration of the peristaltic pump

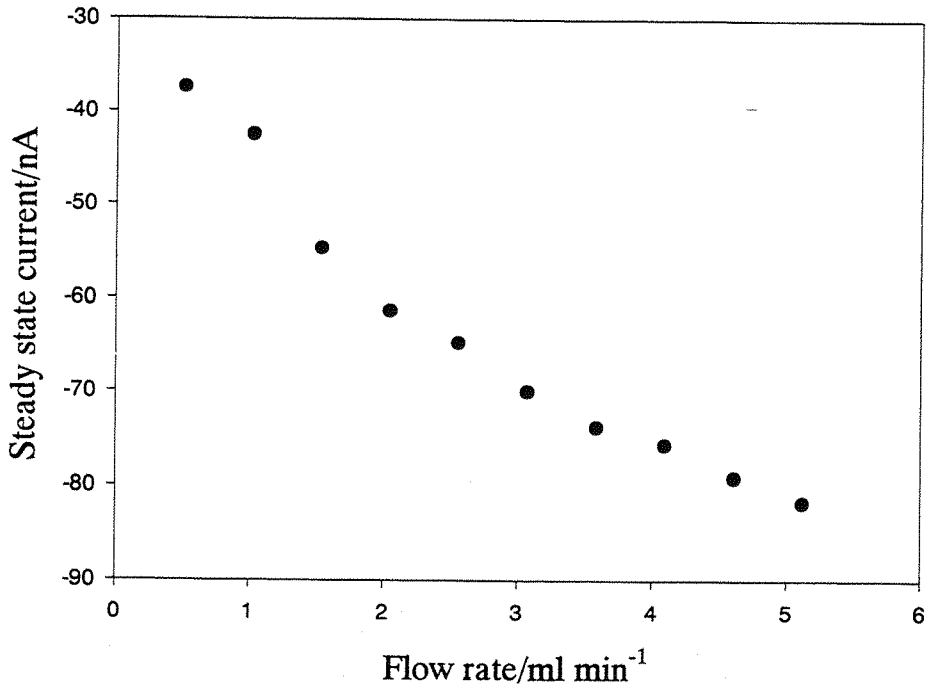

Figure 2.16: Steady state current recorded at a 10 mm Pt microelectrode from a degassed 5 mmol dm^{-3} hexaamine ruthenium (III) chloride, $[Ru(NH_3)_6]Cl_3$ and 0.1 mol dm^{-3} KCl solution.

References

[1] T. G. Leighton, *The acoustic bubble*, Academic Press 1994, p. 101.

[2] M. Bertotti, D. Pletcher, *Analytica Chimica Acta 337* (1997) 49.

3. Physical properties

The aim of this chapter is to report a study of the electrical properties of the ultrasonic device, including the impedance of the transducer, the output power from the generator and to describe the pressure field within and above the cell. These measurements were achieved in order to correlate (see general conclusion chapter 6) the physical properties with the chemical activity within the cell as a function of frequency.

3.1 Impedance

Figures 3.1 and 3.2 show the real and the imaginary parts of the impedance of two systems. In the first system the impedance of the transducer only was measured, whereas in the second system measurement of the impedance of a glass cell attached to the transducer containing 100 ml of solution was achieved. From the peaks of the dotted lines on figure 3.1 and 3.2, resonant frequencies of the transducer could be deduced. When a cell containing 100 ml of liquid is added to the system, the impedance changes as a function of frequency become more complicated. Other resonant frequencies appear, whereas resonant frequencies due to the transducer appear to be reduced.

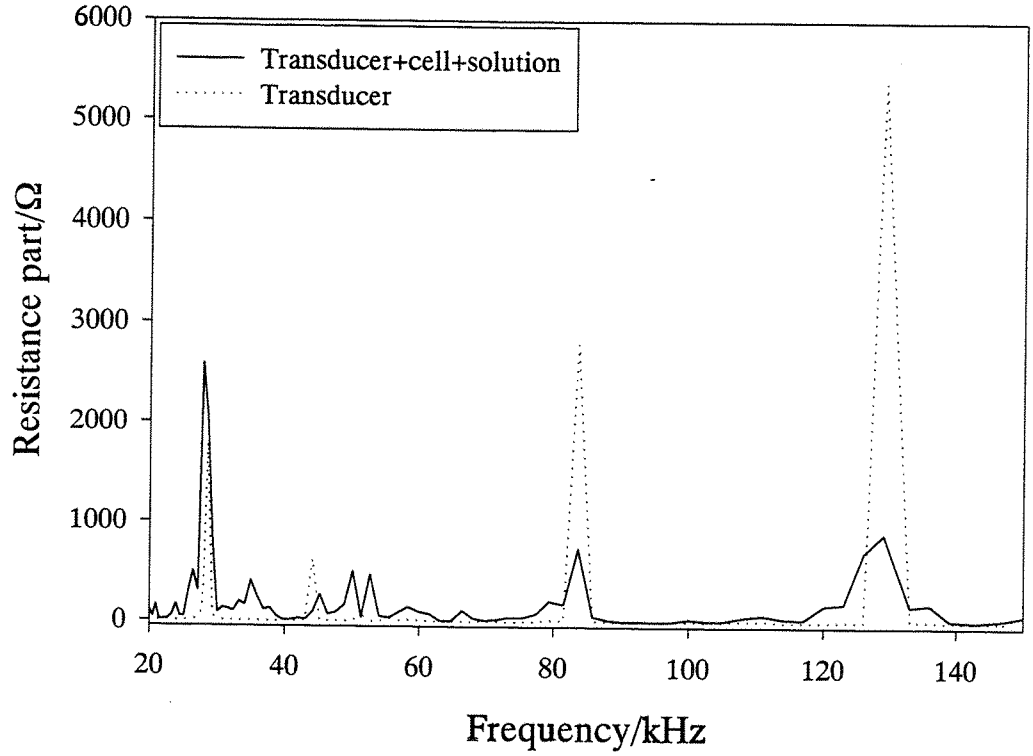

Figure 3.1: The figure shows a comparison of real part of the transducer impedance (solid line) and of the system transducer/cell containing 100 ml of liquid (dotted line) as functions of frequency.

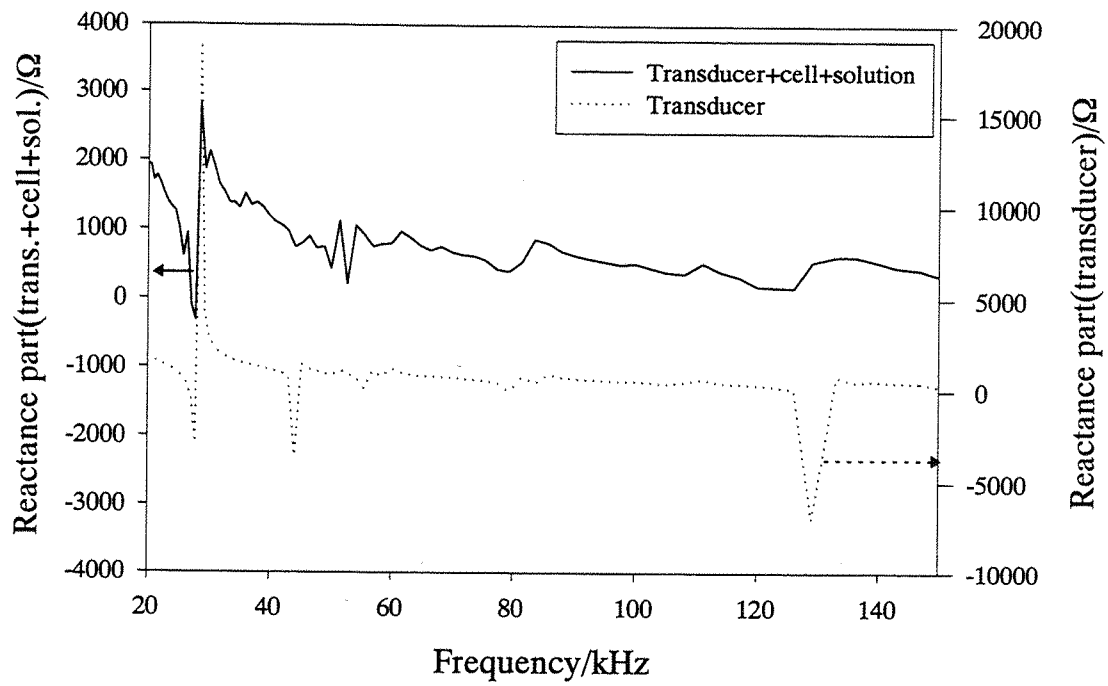

Figure 3.2: The figure shows a comparison of imaginary part of the transducer impedance (solid line) and of the system transducer/cell containing 100 ml of liquid (dotted line) as functions of frequency.

It is not the purpose of this thesis to give a physical interpretation of this phenomenon, but a comparison of these properties with the observable chemical effects will be given in chapter 6.

3.2 Output power

The efficiency of the cell is a function of the applied voltage and the electrical characteristics of the transducer as a function of frequency. In order to attempt to quantify this behaviour calibration of the transducer was undertaken. It is commonly achieved by the use of calorimetry, where the input of energy is proportional to the rise of temperature per unit of time. However, an electrical measurement was preferred in the present case because of the simplicity of the device required. Moreover, a measurement of temperature by a thermocouple could be measured at different points within the reactor, therefore a calorimetric measurement is local and does not reflect the whole system. Contamine *et al.* [1] found that electrical input and output power to and from a generator are proportional. It is also important to consider power consumption against ultimate chemical effect.

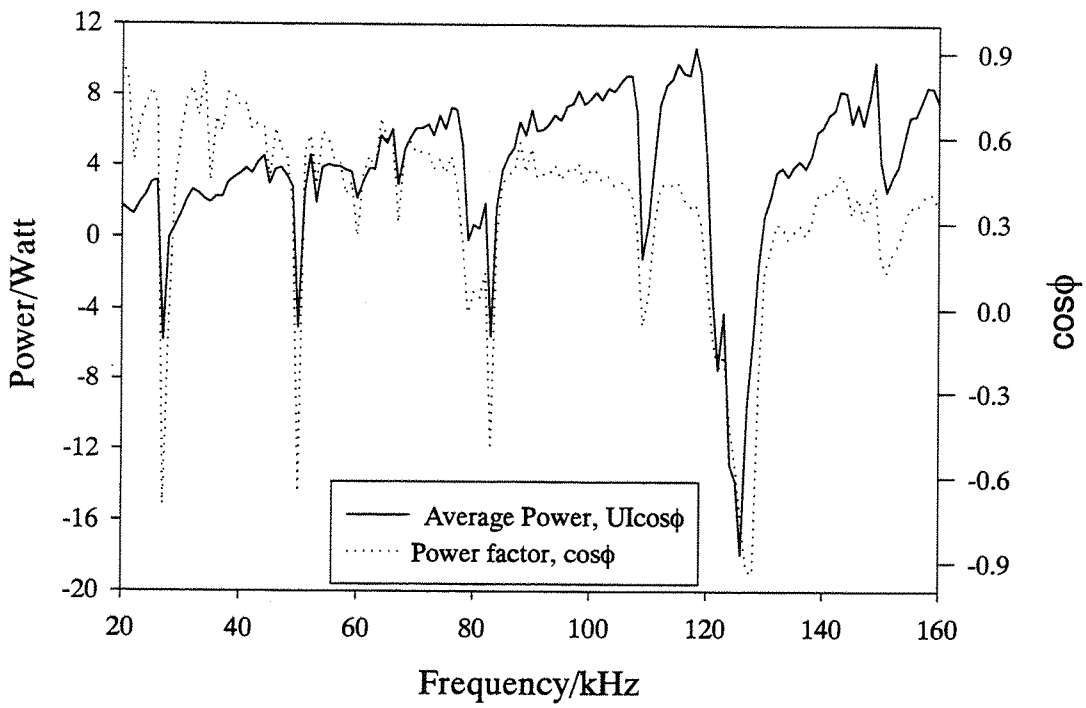

Figure 3.3: Measurement of the output power corresponding to V_{RMS}=90V for the generator.

Figure 3.3 shows the output power from the power amplifier. This measurement was achieved by recording the voltage of the power amplifier and the current circulating through the electrical circuit (see chapter 2.4.3).

The sign of the output power will depend on the behaviour (receptor or generator) of the transducer. The curve showing the variation of the output power with frequency can be explained as follows: Shift of the base line is due to the apparent power (the product of the voltage by the current), whereas actual peaks reflect an increase of the power factor (which is the cosine of the phase angle between the current and the voltage).

Power measurement provide an indication of the system efficiency, however, it appears to be difficult to correlate the output power to the chemical activity as a function of frequency (see chapter 6).

3.3 Audible sound output

Cavitation bubbles, whether of the stable or transient nature, act as secondary sound sources emitting spherical waves. This acoustic emission may be at the driving frequency, f, or at other frequencies, since the bubble will have a resonance frequency and non linear equations govern the motion of the bubble.

Esche [2] was the first to record spectra of the sound output for different transducers (covering frequencies from 3 kHz to 3.3 Mhz). Depending on the drive power, he found that the spectrum may contain lines at harmonics of the driving frequency, $n*f$, at subharmonics, f/n or at ultraharmonics $(n+1/2)*f$. Sound emission during transient cavitation is also characterised by a broadband continuum. The continuum is attributed to the rapidly changing bubble radius. In the present study, a spectrum of the sound output was not obtained, but the acoustic intensity level of the sound emission was measured by a microphone which picked up all the waves of frequency from 20 Hz to 20 kHz corresponding to the audible sound. Figure 3.4 shows

that emission of audible sound occured at low driving frequencies (lower than 85 kHz). Moreover, it can be noticed that the sound output increases drastically at the resonant frequency of the transducer.

These results have to be compared with pressure measurements within the cell. It should be noticed that at 24 kHz, scattering due to harmonics and subharmonics of the driving frequency were observed on the signal picked up by the hydrophone (see chapter 2, figure 2.8), whereas at 122 kHz, only sinusoidal variation of the pressure at the driving frequency was observed (see chapter 2, figure 2.9). Subharmonic emissions at 24 kHz shows that transient cavitation occurs within the cell.

The general decrease of acoustic emissions from bubbles with increasing driving frequencies is thought to be due to limitations of the microphone, which has a linear response only up to 20 kHz. Therefore emissions at harmonics of the sonication frequency are not picked up.

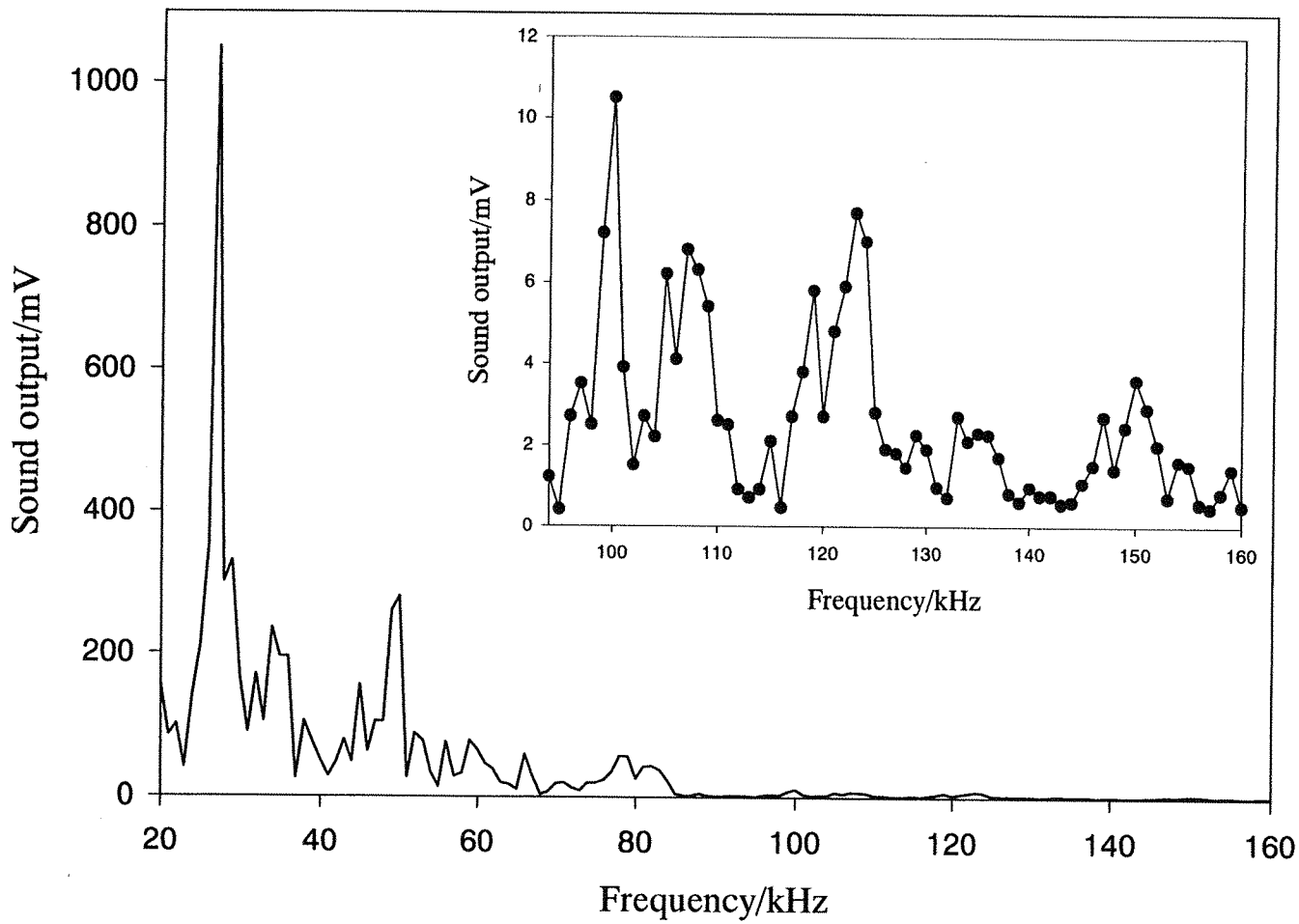

Figure 3.4: The figure shows a plot of the sound output as a function of frequency. The insert represents an enlargement of the measurements corresponding to the 90-160 kHz frequency range.

3.4 Pressure measurements

3.4.1 Radial and axial variations

Pressure across the cell was measured by moving a hydrophone along the radius (figure 3.5) and the axis (figure 3.6) of the cell. Clearly characteristic patterns in the pressure field can be seen.

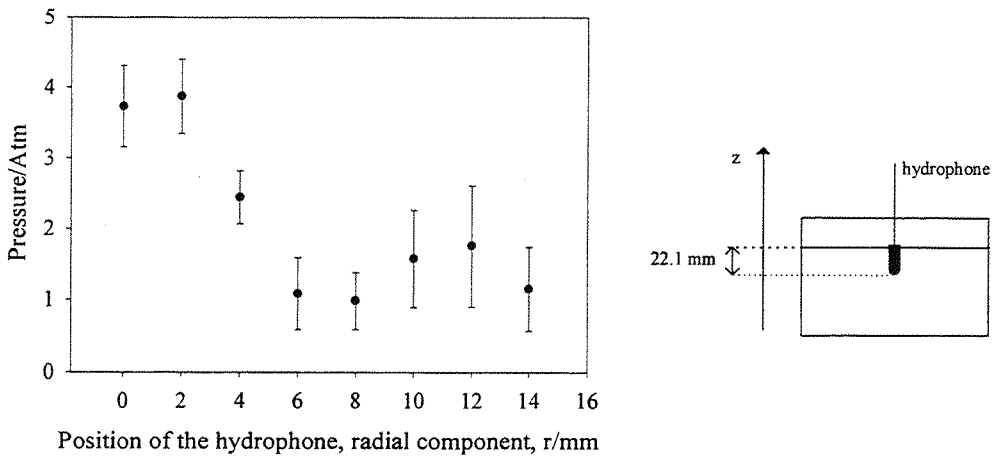

Figure 3.5: Variation of pressure within the cell in radial direction during the irradiation at 122 kHz of a 10 mmol dm^{-3} HCl and 0.1 mol dm^{-3} NaCl solution. The origin of the radial component axis corresponds to the centre of the cell.

As shown on figure 3.5, variations of pressure in radial direction are periodic, but these variations are less important further away from the cell axis. Maximum intensity was found close to the axis of the cell. Such a distribution is very similar to those found in the study of mass transfer [3] . Moreover, these variations in pressure are generally expected for a circular cell design with modal functionnality.

Similarly, the pressure appears to vary periodically along the axis of the cell. Height of pressure maxima are close, showing no significant absorption from the solution. These results are in agreement with a standing wave pattern model. The acoustic model (see paragraph 1.6) predicts pressure maxima in a ring pattern as viewed from above the cell and equidistant bands if viewed from the side.

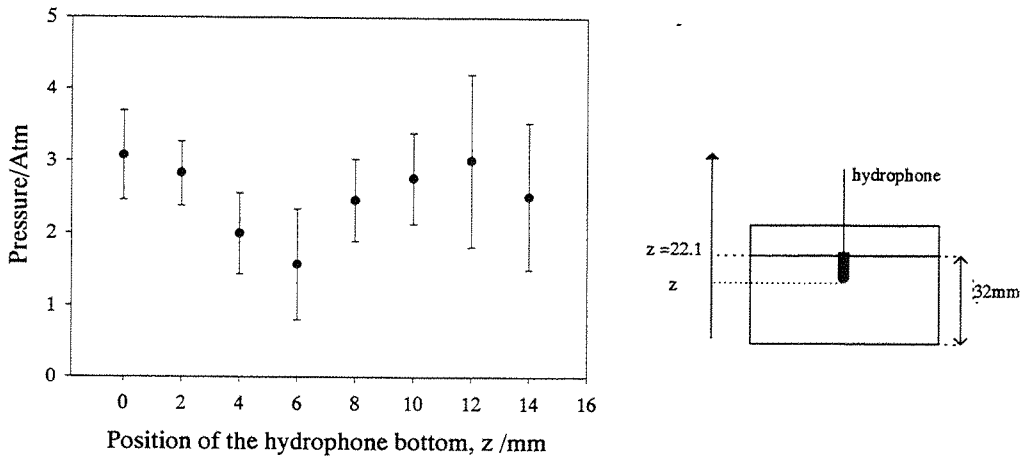

Figure 3.6: Axial profile of pressure variation within the cell during the irradiation at 122 kHz of a 10 mmol dm^{-3} HCl and 0.1 mol dm^{-3} NaCl solution

3.4.2 Frequency dependence

In this study, the hydrophone was placed on the axis of the cell and 3.5 cm away from the liquid/air interface. A local measurement of the pressure as a function of frequency was then achieved. Figure 3.7 shows the experimental data, theoretical predictions obtained by considering equation (16) (page 24, chapter1) are also reported on this graph.

As seen on the figure 3.7 peaks of pressure are observed at discrete frequencies. Moreover, predictions from a theoretical pressure field seems to agree reasonably well with the experimental data. Small differences between experimental and theoretical pressure as a function of frequency could be explained by the fact that measurements and calculations were not achieved for the same position within the cell.

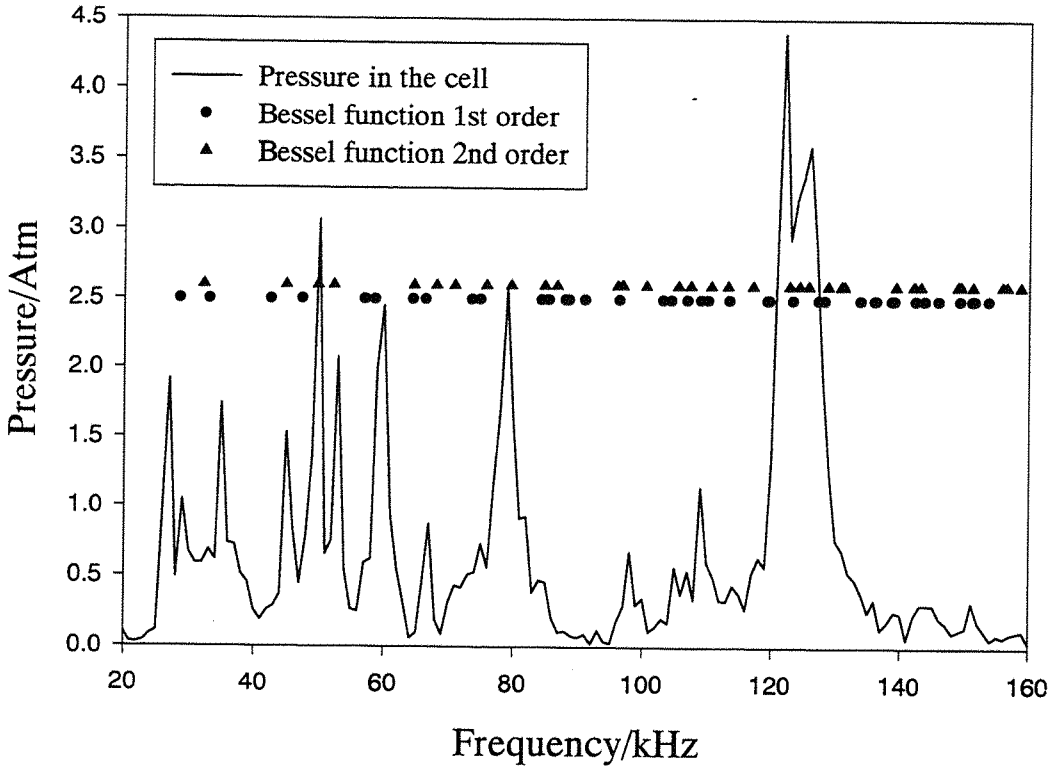

Figure 3.7: Local measurement of the pressure as a function of frequency. The hydrophone was positioned along the axis of the cell and 3.5 cm away from the liquid/air interface. 100 ml of solution was irradiated at 25 °C. Previsions from theoretical calculations are also reported by the scatter plots.

It should be noticed that pressure measurements are local whereas light emission or reaction rate determination reflect the activity of the whole cell. As seen in figure 3.8, depending on the mode (and therefore on the frequency) the hydrophone could be located or not on a pressure maximum of the standing wave pattern or not.

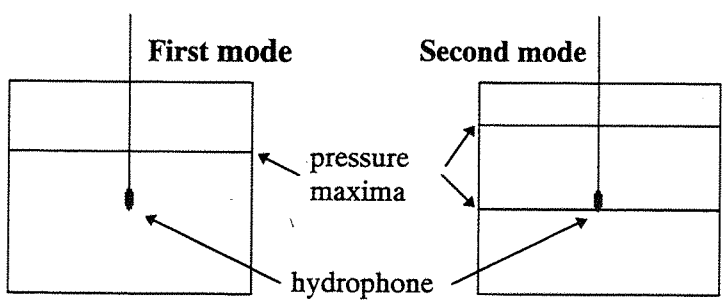

Figure 3.8: The figure shows relative positions of the hydrophone and pressure maxima for the two first possible standing wave field.

The comparison of pressure as a function of frequency with the chemical activity will be further discussed in chapter 6.

References

[1] F. Contamine, A. M. Wilhelm, J. Berlan, H.Delmas, *Ultrasonics sonochemistry 2* (1995) 43.

[2] R. Esche, *Acustica 2* (1952) AB 208.

[3] F. Faid, F. Contamine, A. M. Wilhelm, H. Delmas, *Ultrasonics Sonochemistry 5* (1998) 119.

4 Sonoluminescence

For many years, interest in sonoluminescence has led to numerous studies of this phenomenom [1-4]. However, in most cases, the articles consist of postulated mechanisms concerning the origin of this phenomenom. Some of these studies are based on observations of individual bubbles [5, 6]. No papers are devoted to a simultaneous study of sonoluminescence and chemical activity. Electrochemical methods [7] are more often used for the characterisation of high activity regions within ultrasonic reactors. These methods are based on the measurement of the mass transport limited current of a reversible electrochemical system under pseudo-stationary conditions and lead to the calculation of mass transfer coefficients. Even though electrochemical methods are powerful in their ability to determin active local regions within the liquid, they do not give a picture of the global sound field within the cell. In this chapter, emission of light by a sonicated solution was preferred to investigate energetic regions within the reactor and for the determination of the most efficient irradiation frequency.

4.1 Pictures

Pictures taken during the irradiation of a solution were used to visualise the zones where sonochemical reactions were thought to be the most active. Pictures of the active zones were taken using solutions of luminol. Alkaline solutions of this compound have been known for quite sometime to enhance light emission compare to sonoluminescence observed in water [8, 9].

The increase in intensity is so high that sonochemilumiscence of luminol is visible to the naked eye within a dark room. This light enhancement is caused by emission from the excited state of the final product 3-aminophtalate. The principal mechanism that is proposed for sonochemiluminescence of luminol in aqueous alkaline solutions involves sonochemical co-oxidation of the luminol anion and an oxygen derived species by oxidising agent produced by cavitation[10].

4.1.1 Experimental scale

In this particular experiment, hydrogen peroxide and EDTA were added to the solution of luminol to improve the resolution of the sonoluminescence pictures [11]. Previous studies showed that hydrogen peroxide had a dynamic effect on the intensity of the emitted light. However, light emission from solutions containing luminol and hydrogen peroxide is produced by divalent transition metal cation that catalyse a non-sonochemical luminescence [12]. Hence, a chelating agent complexing the metal cations, EDTA, was added to solution to prevent this catalytic effect.

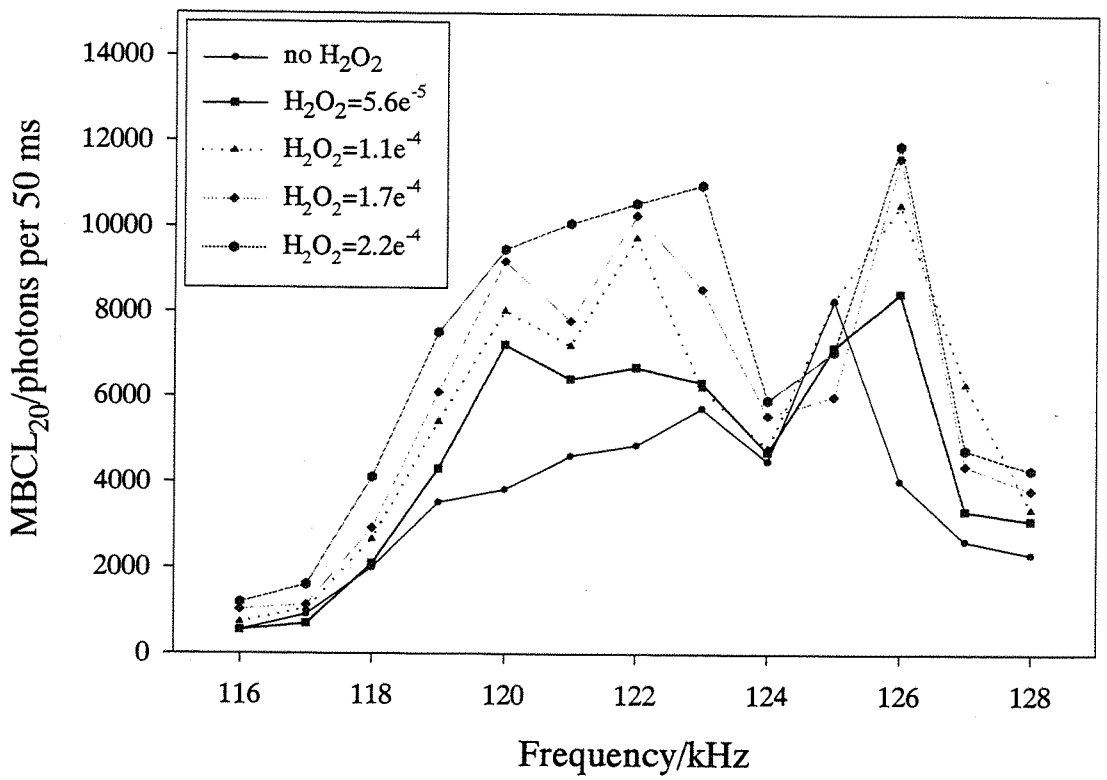

Figure 4.1: Effect of hydrogen peroxide on the sonochemiluminescence of an 1.0 mmol dm^{-3} luminol, 50 mmol dm^{-3} Na_2CO_3 and 5 mmol dm^{-3} EDTA solution.

Experiments carried out by Wilson [13] on the influence of hydrogen peroxide were repeated in the present work. Figure 4.1 shows the chemiluminescence of a 1.0 mmol dm^{-3} luminol solution as a function of frequency for different concentration of hydrogen peroxide in presence of 5 μmol dm^{-3} EDTA. Addition of hydrogen peroxide clearly increases light emission over the studied range of concentrations. Moreover a

comparison of the first curve on figure 4.1 with the sonochemiluminescence of a solution without EDTA (see figure 4.6) shows that EDTA also has a positive effect on light emission.

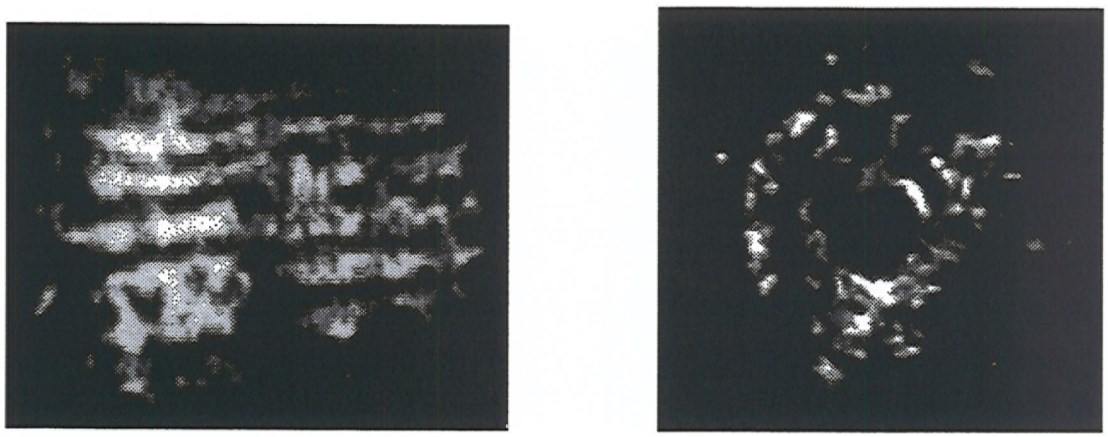

Figure 4.2: Sonochemiluminescence of a 100 ml solution containing 1.0 mmol dm^{-3} luminol, 50 mmol dm^{-3} Na_2CO_3, 5 mmol dm^{-3} EDTA and 0.33 mmol dm^{-3} H_2O_2 solution. Vertical view of the cell was taken at 119.1 kHz, while the picture, taken vertically above the cell, shows the active region within a cell driven at 150.2 kHz

Figure 4.2 shows the commonly observed patterns af light emission recorded for a glass cell containing an alkaline luminol/EDTA/H_2O_2 solution. Clearly characteristic patterns of light can be seen. On the vertical view, equidistant bands of light can be seen, while the picture taken from the top of the cell shows circular patterns. These are discussed in the following paragraph.

4.1.2 Scale-up

In this section, the sonicated volume was increased by a factor of ten: one litre of a 1.2 mmol dm^{-3} luminol and 50 mmol dm^{-3} Na_2CO_3 was irradiated in the perspex cell. The emitted light patterns were recorded.

As seen in figures 4.3 and 4.4, the resolution of the pictures is considerably better than for previous experiments. This can be explained by the use of a perspex cap which acts as a rigid boundary and reduced scattering due to surface waves formed at the solution/air surface. Another explanation consists in the fact that the light intensity emitted by a one litre solution is more intense than light emitted by 100 ml of the same

solution. However, this assumption was not confirmed by photoncounting as shown on figures 4.5 and 4.6.

From these pictures it can be seen that for a cylindrical cell characteristic patterns exist. These consist of equidistant bands on vertical views of the cell and circles on pictures taken from the top of the cell. However, it was noted that the number of circles and bands depends on the driving frequency. In fact, the number of luminous bands goes up when the frequency is increased and hence, more of the solution will be active. These observations are consistent with a "standing wave pattern" as predicted by the three dimensions geometry and acoustics of the system (see chapter 1.6).

Observations from the side of the cell (figure 4.3) confirm results from Pinoir and Pouradier [14]. Thus, they found that in a standing wave pattern bands of light appeared perpendicular to the acoustic beam, $\lambda/2$ spaced from each other. Leighton and coworkers [15] have proved that this distance corresponds to the antinode-antinode spacing and the sonoluminescence is aligned with the pressure antinodes. Hence, luminescence is thought to be produced by bubbles of smaller than resonance size: In a focused acoustic field bubbles below resonance size travel to the focal pressure antinodes through the primary Bjerkness force [16]. However, due to the high bubble density at antinodes, interaction between bubbles is considerable. The sound field experienced by a bubble is modified through the secondary Bjerkness forces excerced by the other bubbles. Hence, the first bubble oscillates violently until it collapses. Moreover, it was shown that emission of light is correlated to bubble collapse [5].

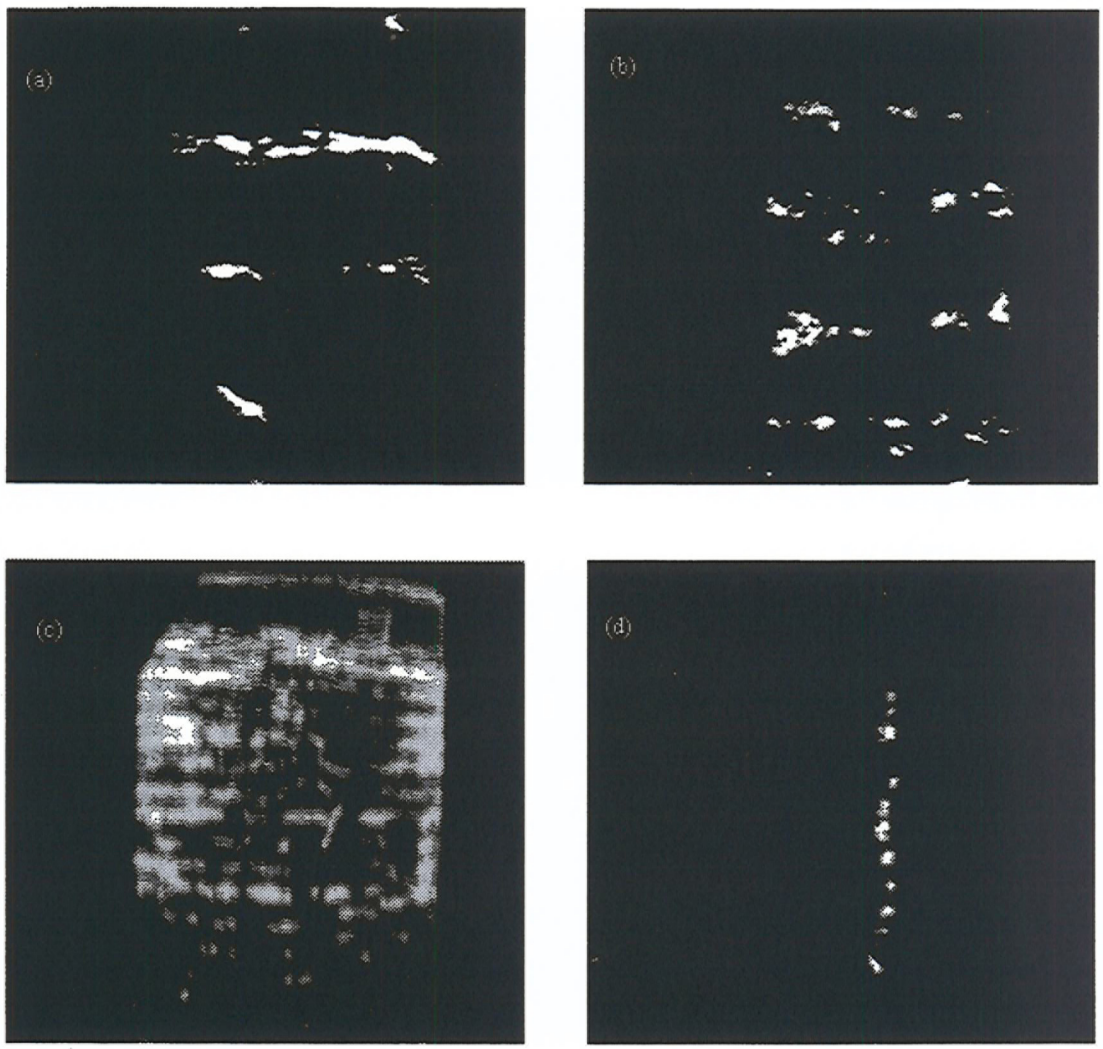

Figure 4.3: Sonochemiluminescence of a one litre solution containing 1.2 mmol dm^{-3} luminol and 50 mmol dm^{-3} Na_2CO_3 recorded by an image intensified CDD camera placed horizontally on the side of the cell. Solution was sonicated at: (a) 20.78 kHz, (b) 22.52 kHz, (c) 92.03 kHz, (d) 100.82 kHz.

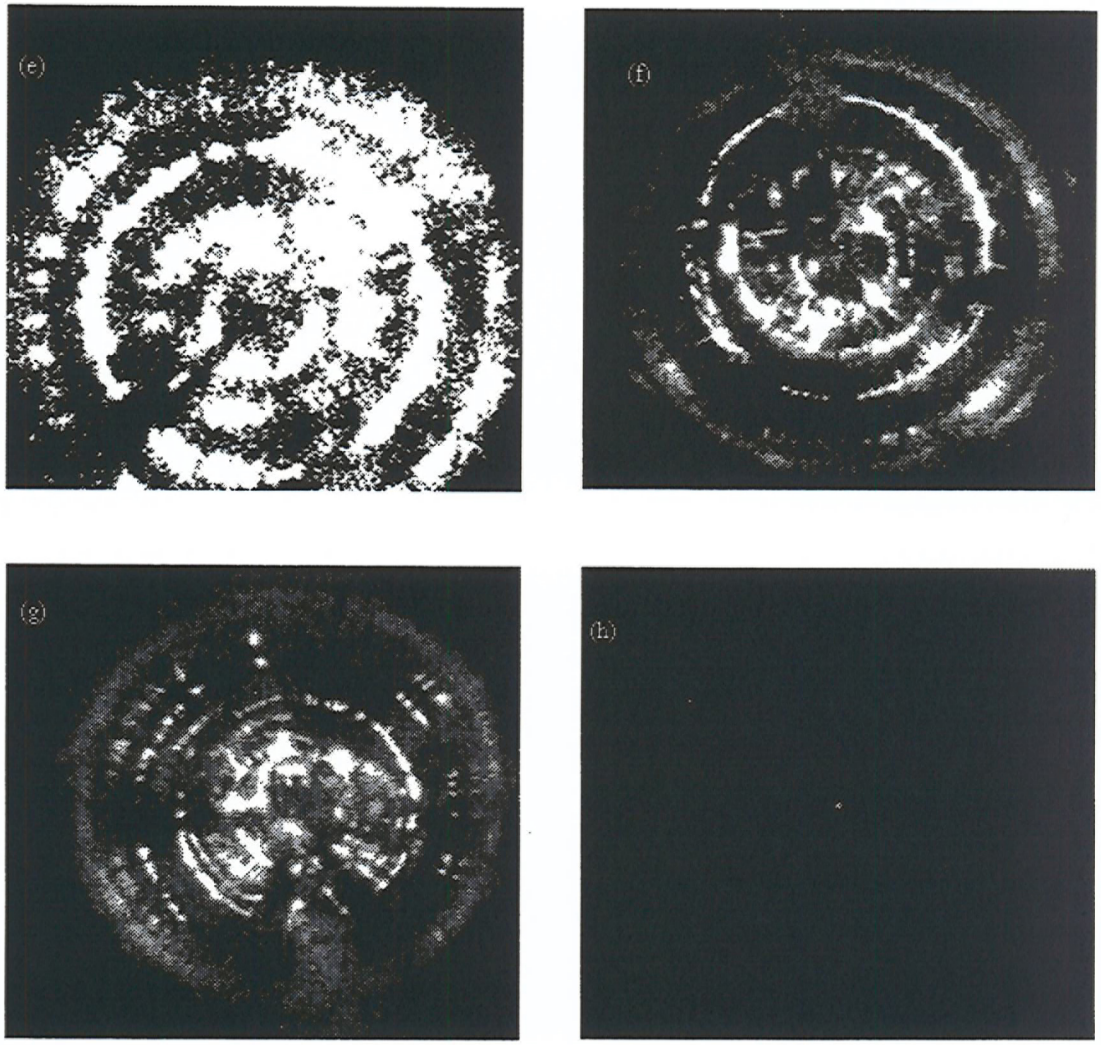

Figure 4.4: Sonochemiluminescence of a one litre solution containing 1.2 mmol dm^{-3} luminol and 50 mmol dm^{-3} Na_2CO_3 recorded by an image intensified CDD camera. Camera was placed above the cell during irradiation at: (e) 49.70 kHz, (f) 49.88 kHz, (g) 74.90 kHz and (h) 132.6 kHz

Figure 4.4 shows a set of characteristic rings due to the Bessel function nature of the pressure field in radial direction. Discontinuity in rings can be due to imperfections of the cell or non-perfect transducer oscillation. Such a defect leads to an angular dependence on sound field and higher order Bessel functions to explain the radial character of the system. This explains the absence of a luminous spot in the centre of the cell on most of the pictures.

The spatial distribution of the light emission was hence determined. In the next section quantification of the light output from the cells employed using a photoncounter is reported.

4.2 Photoncount

4.2.1 Experimental scale

4.2.1a Sonoluminescence

Emission of light from 100 ml of a 50 mmol dm^{-3} Na_2CO_3 solution was investigated as a function of frequency over a range of 20 kHz to 160 kHz. Figure 4.5 shows the average emission of photons per 50 ms. The light intensity appears to be strongly dependent on the sound frequency employed. Light emission occurs at discrete frequencies consistent with the modal functionality of the system. Over a large range of low frequencies (until 77 kHz), no light was observed. At higher frequencies, four major peaks of light emission were observed. High luminescence was specially observable from 119 kHz to 128 kHz with a maximum at 122 kHz.

This 119-128 kHz frequency range does not correspond to the resonant frequency of the transducer (25 kHz). At 25 kHz the geometry of the piezo-electric components is optimal, but at this frequency the production of hydroxyl radicals appears to be low. This could be due to a poor response of the glass cell containing the solution. To be efficient, frequency has to correspond to a vibration mode of both transducer and system cell-solution.

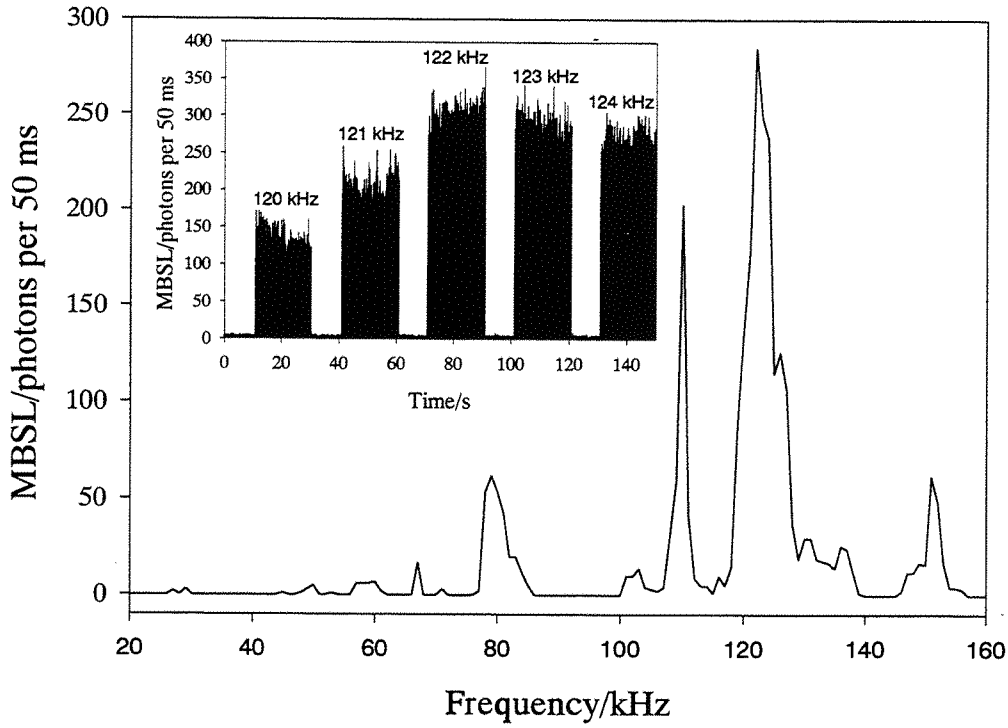

Figure 4.5: The figure shows the emission of light from 100 ml of a 50 mmol dm^{-3} Na_2CO_3 as a function of frequency. The insert reproduces row data as obtained from the software. As seen on the insert, photoncounting per 50 ms was achieved during 20 seconds under sonicated conditions and then 10 seconds under silent conditions. During the silent period, the frequency of the transducer driving generator is increased by 1 kHz and then light intensity during the irradiation at the new frequency was measured. An average of these counts over 20 seconds was used as the final light emission value in the main figure.

4.2.1b Sonochemiluminescence

It is a common practice to employ alkali solutions of luminol to enhance light output from cavitating media. Figure 4.6 shows the influence of frequency on the sonochemiluminescence of a 100 ml solution containing 1.2 mmol dm^{-3} luminol and 50 mmol dm^{-3} Na_2CO_3. As expected the intensity of the emitted light was found to be much greater than for an alkaline water solution. Light emission was enhanced by ca. 15 times.

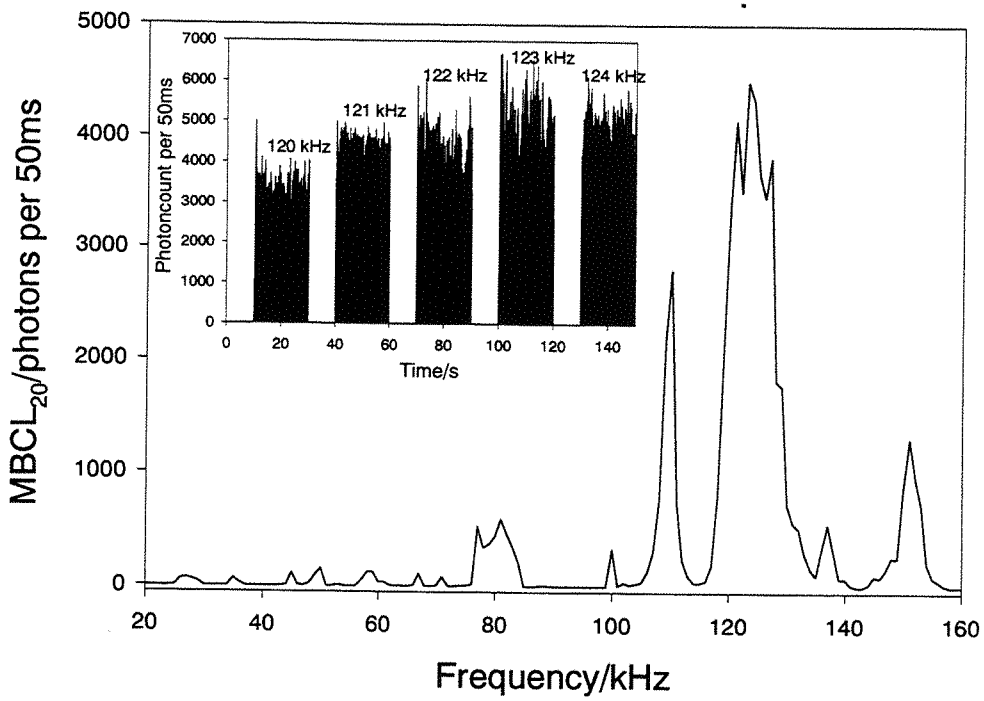

Figure 4.6: The influence of frequency on the sonochemiluminescence of a 100 ml solution containing 1.2 mmol dm^{-3} luminol and 50 mmol dm^{-3} Na_2CO_3

The shape of the sonochemiluminescence curve as a function of frequency was found to be the same as for sonoluminescence (see figures 4.5 and 4.6). Only small changes were observable. These variations can be due to either chemical change of the solution composition or small fluctuations of the solution volume.

4.2.2 Scale-up

Similar experiments were performed in the 'scale-up' cell. Irradiation of two 1.2 mmol dm^{-3} luminol and 50 mmol dm^{-3} Na_2CO_3 solution was carried out in the perspex cell. In the first experiment 100 ml of solution was sonicated, whereas the second experiment was performed using one litre of solution. Sonoluminescence as a function of frequency was recorded in both case.

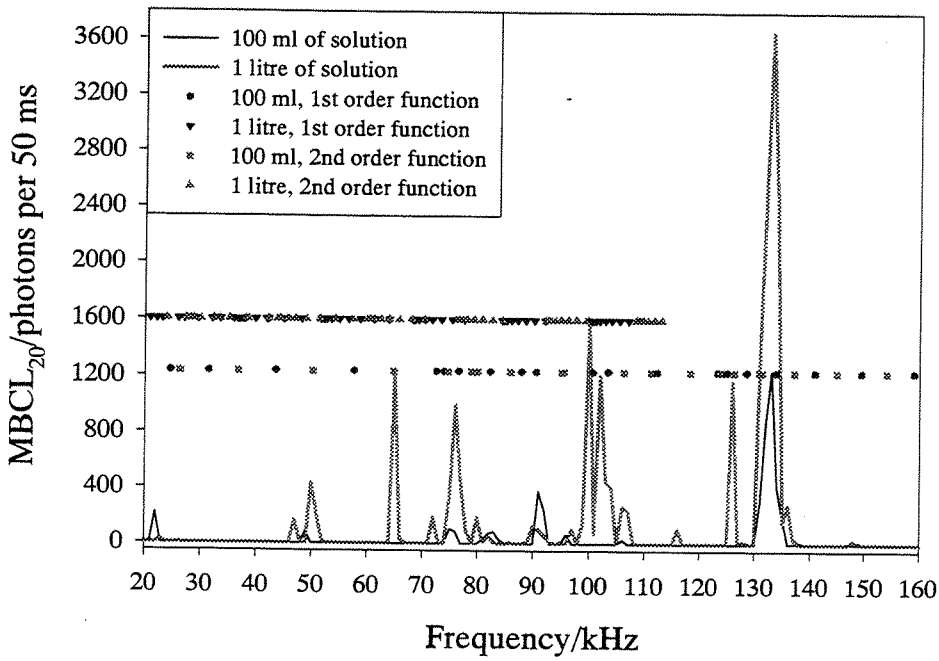

Figure 4.7: Sonochemiluminescence of a 1.2 mmol dm^{-3} luminol and 50 mmol dm^{-3} Na_2CO_3 solution as a function of frequency. Experiments were carried out in a cylindrical perspex cell either with one litre or 100 ml of solution.

As shown on figure 4.7, the sonochemiluminescence output of the cell as a function of frequency. Two different cell volumes were employed in these experiments, 100 ml and 1000 ml respectively. It can be seen that frequencies at which 100 ml of solution emit light will also be efficient for the sonochemiluminescence of a one litre solution and in both cases maximum sonochemiluminescence occurs at the same frequency, 132 kHz. On the other hand peaks of light were more numerous in the case of the one litre solution.

For both experiments the counter was located at the same position. The collection efficiency of the photoncounter is difficult to estimate, but considering solid angles (see figure 4.8), the collection efficiency of the counter is thought to be higher for larger cell volumes.

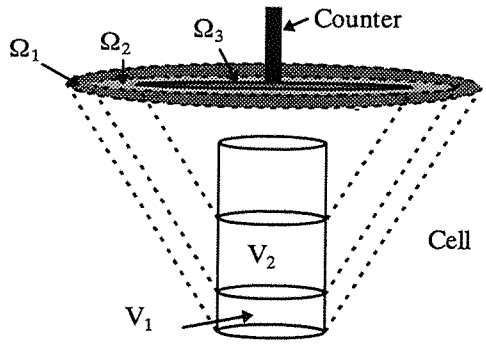

Figure 4.8: The figure shows solid angles of the light emission from two solutions, V1 and V2

Maximum light emission recorded from a one litre solution was three times more intense than for the 100 ml solution, however, at equivalent efficiency intensity should be proportional to the sonicated volume. Therefore it seems that the system is less efficient for a one litre solution.

As reported in paragraph 4.1.2, the standing wave pattern seems to fit quite well with the results. Therefore expected maxima corresponding to a standing wave field were plotted in figure 4.7. These maxima form a quasi continuum in the case of the one litre solution. In other words the cell design and the volume of the solution are no more restrictive in the determination of efficient frequencies. Light emission from the solution is expected to be determined only by the vibration modes of the transducer. In the case of the 100 ml solution, peaks of light result from a combination of efficiency of both transducer and cell containing solution.

4.3 Conclusion

Sonochemiluminescence is found to be an effective method to characterise active zones within a cell. Activity, which is strongly dependent on the applied frequency, appears to be concentrated on rings perpendicular to the acoustic beam. These observations are in agreement with predictions given by a simple acoustic model. At last scale-up experiments show that for the present cell device an increase of the sonicated volume provokes an efficiency loss.

References

[1] N. Marinesco, M. Reggiani, *C. r. hebd. seanc. acad. sci. 200* (1935) 548.

[2] A. J. Walton, G. T. Reynolds, *Advances in Physics 33* (1984) 595.

[3] D. J. Walton, S. S. Phull, D. M. Bates, J. P. Lorimer, T. J. Mason, *Electrochimica acta 38* (1993) 307.

[4] M. Degrois, P. Baldo, *Ultrasonics 12* (1974) 25.

[5] S. J. Putterman, *Scientific American 272* (1995) 32.

[6] B. P. Barber, C. C. Wu, R. Lofsted, P. H. Roberts, S. J. Putterman, *Physical Review Letters 72* (1994) 1380.

[7] F. Faid, F. Contamine, A. M. Wilhelm, H. Delmas, *Ultrasonics Sonochemistry 5* (1998) 119.

[8] E. N. Harvey, *J. Amer. Chem. Soc. 61* (1939) 2392.

[9] K. Negishi, *J. Phys. Soc. Japan 16* (1961) 1450.

[10] J. Lind, G. Merenyi, T. E. Eriksen, *J. Am. Chem. Soc. 105* (1983) 7655.

[11] H. N. McMurray, B. P. Wilson, *J. Phys. Chem. A 103* (1999) 3955.

[12] L. L. Klopf, T. A. Nieman, *Anal. Chem. 55* (1983) 1080.

[13] B. P. Wilson, *Department of Materials Engineering*, University of Wales, Swansea 1998.

[14] R. P. a. J. Pouradier, *J. Chim. Phys. 44* (1947) 261.

[15] T. G. Leighton, M. J. W. Pickworth, A. J. Walton, P. P. Dendy, *Phys. Med. Biol. 33* (1988) 1239.

[16] T. G. Leighton, *The acoustic bubble*, Academic Press 1994, p. 101.

5 Measurement of reaction rate

Interest in pollutant degradation has led to the study of ultrasonic irradiation of numerous chemical contaminants. Substrates such as potassium iodide [1-3], phenols [4, 5], chlorinated hydrocarbons, esters [6-10] are degraded when they are sonicated. Moreover, during ultrasonic degradation of these compounds conversion yields of the impurities were found to be very efficient under proper conditions. As an example Trabelsi *et al.* [11] obtained by sonoelectrochemistry conversion up to 95% for the oxidation of phenol into acetic and chloroacrylic acids.

The aim of this chapter is to report the results of a study on the influence of the irradiation frequency on the chemical reaction rate of two reactions. Additionally the influence of hydrogen peroxide on degradation is also reported.

5.1 Degradation of Meldola blue

5.1.1 Influence of hydrogen peroxide

The change in Meldola blue concentration was followed for three experiments over the period of one hour. All experiments were carried out with 100 ml of a 0.1 mmol dm^{-3} Meldola blue solution containing 10 mmol.dm^{-3} HCl and 0.1 mol dm^{-3} NaCl. In the first experiment hydrogen peroxide (10 mmol dm^{-3}) was added to this solution and the solution was sonicated. In the second experiment ultrasound was applied to the solution without addition of hydrogen peroxide. In the third experiment hydrogen peroxide was added to the solution and absorbance of this solution was followed during one hour at 570 nm under silent conditions.

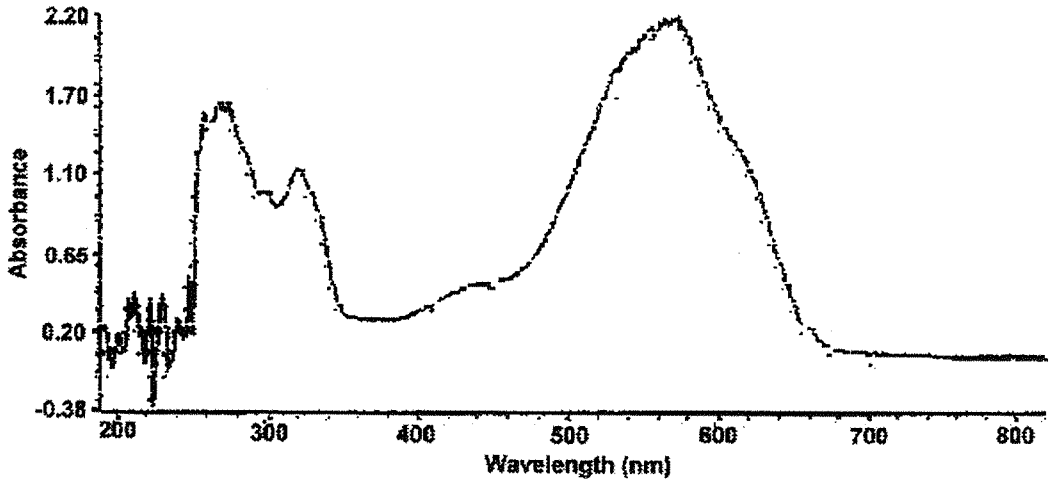

Figure 5.1: UV-spectrum of a 0.1 mmol dm^{-3} Meldola blue, 0.1 mol dm^{-3} NaCl and 10 mmol dm^{-3} HCl solution.

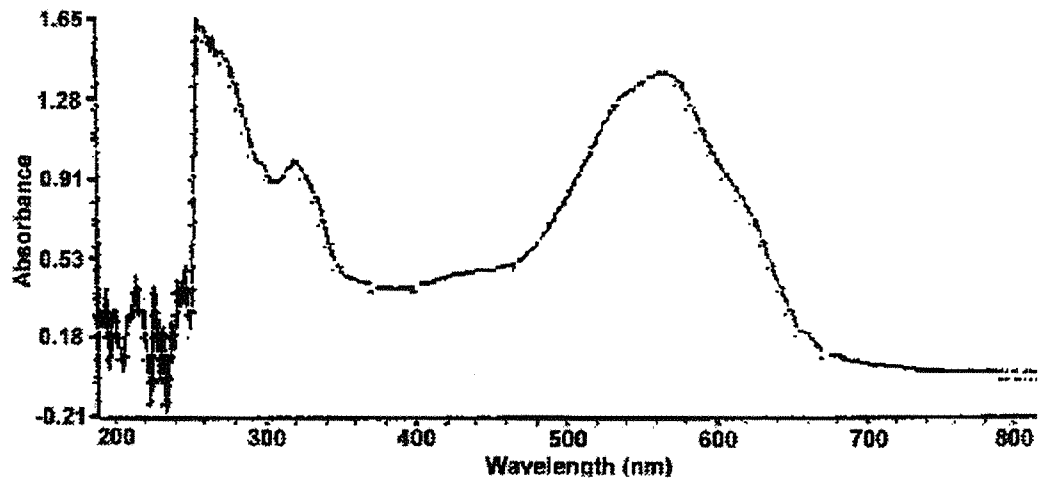

Figure 5.2: UV-spectrum of a 0.1 mmol dm^{-3} Meldola blue, 0.1 mol dm^{-3} NaCl and 10 mmol dm^{-3} HCl solution after irradiation of 100 ml during one hour at 125 kHz.

Figures 5.1 and 5.2 shows the effect of ultrasound on the uv-spectrum of a Meldola blue solution. The decrease in absorbance at λ= 570 nm after irradiation was attributed to the destruction of one benzeic ring in the first step of the degradation.

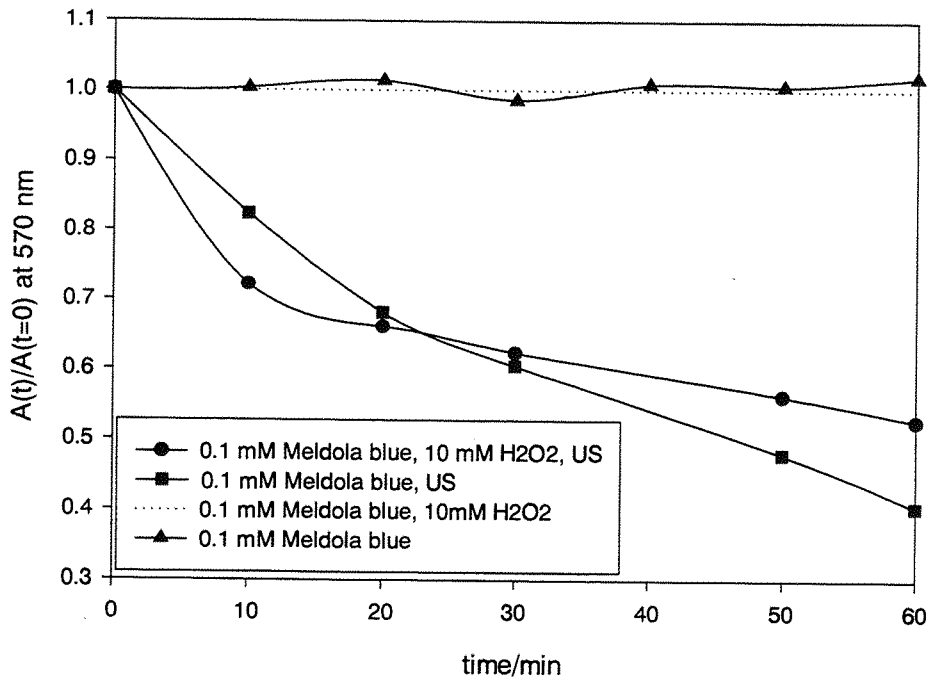

Figure 5.3: Influence of hydrogen peroxide and ultrasound on the degradation of Meldola blue at 25°C. Irradiation was performed at 125.7 kHz on 100 ml solution.

Figure 5.3 shows the normalised absorbance of the solution as a function of time at 570 nm. Under silent conditions no variation of the concentration was observed whereas the application of ultrasound provoked a regular degradation of Meldola blue. However, the addition of hydrogen peroxide to a sonicated solution did not significantly catalyse the reaction and enhance the rate of degradation. These results imply that the most probable chemically active species are hydroxyl radicals produced by ultrasound and not the hydrogen peroxide itself within a solution containing no monovalent metal ions. The second hypothesis is that Meldola blue is degraded by pyrolysis (thermal degradation).

5.1.2 Ultrasonic degradation

To keep the volume of solution in the cell constant, each time a sample was taken, the same amount of solution without Meldola blue was added. In such a way, modifications of the irradiation condition due to a variation of the liquid height were

minimised. The value of $A_{modified}$ (cf appendix) in graph 5.4 takes into account the modifications in analysis due to this dilution:

$$A_{modified} = A_{measured} \times \left(\frac{V_{sol}}{V_{Sol} - V_{sample}} \right)^{n} \qquad \text{equation (1)}$$

where $A_{measured}$, n, V_{sol} and V_{sample} represent absorbance of the sample, the number of dilution, the volume of solution in the cell (100 ml) and the volume of the sample (1 ml respectively).

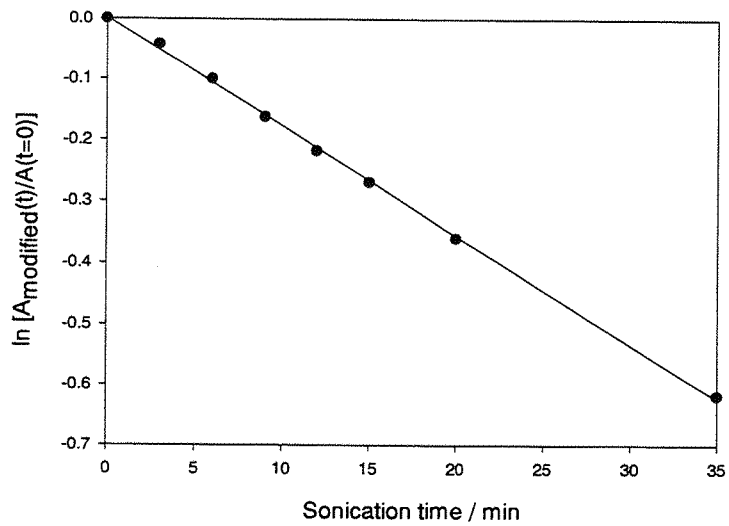

Figure 5.4: First order decay plot of Meldola blue degradation. Irradiation of a 0.1 mmol dm^{-3} Meldola blue solution in 10 mmol dm^{-3} HCl and 0.1 mol dm^{-3} NaCl at 126.0 kHz. $A_{modified}$ is defined by equation (1).

Figure 5.4 shows an example of the observed linearly decrease of ln $A_{modified}$ with sonication time. The ultrasonic degradation of Meldola blue follows apparent first order kinetic. Hence, a first order rate constant was determined from the slope of this plot. In the same manner the first order rate constant was calculated as a function of frequency for the cell employed. This kinetic law is not unusual, first order rate constants or initial rates are often used in literature to describe degradation kinetics [4, 5, 12, 13]

The following table shows the reproducibility of the rate constant measurement for the irradiation of the Meldola blue solution at 124.0 kHz.

Measurement	Rate constant (min^{-1})
1st	0.0077
2nd	0.0107
3rd	0.0080
4th	0.0082

Rate = 0.0087 ± 0.0025

It can be noted that the reproducibility of measurements was not ideal. However, the measurements were very sensitive to the volume of solution in the cell (a 0.1 ml magnitude variation provokes a significant change of the measured rate). Nevertheless the precision was enough to compare the variations of the reaction rate constant as a function of frequency. Figure 5.5 shows the variation in the degradation rate as a function of frequency compared to $MBSL_{50}$.

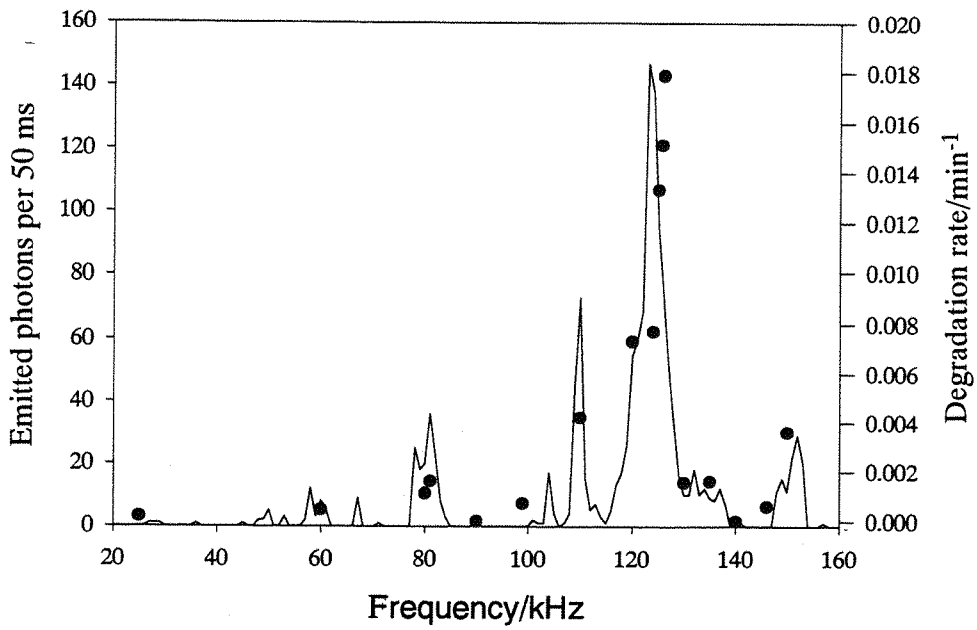

Figure 5.5: Black points represent the degradation rate of Meldola blue as a function of frequency during the irradiation of a 0.1 mmol dm^{-3} Meldola blue solution in 10 mmol dm^{-3} HCl and 0.1 mol dm^{-3} NaCl. The solid line shows the sonoluminescence of a 10 mmol dm^{-3} HCl and 0.1 mol dm^{-3} NaCl solution during the irradiation of 100 ml.

The degradation of Meldola blue was found to be strongly dependent on frequency. In particular at 125 kHz-126 kHz, chemical activity was much more important than at other frequencies. Two others efficient frequency ranges were observed at 80 kHz and 150 kHz.

The influence of frequency on chemical rate has been studied by other workers [5, 11, 14, 15]. However, only a comparison between high and low frequency has been performed. In these studies high frequencies were found to be much more efficient than low frequencies [5, 16, 17]. Petrier *et al.* attributed frequency dependance of rate on the ability of chemical species to exchange from the bubble interior: At low frequencies the life-time of bubbles is longer and oxidative species cannot escape from the bubble to react with impurities in solution, while at higher frequencies the collapse of the bubbles release these oxidative species into the solution. However, the present results show that a study of the chemical activity as a function of frequency should not only compare low and high frequency but also has to be carried out over a large frequency range. The exact reason is not known, but it appears that sonoluminescence, which for multiple bubble systems involve $OH^{\bullet}$, can be used to follow the activity of a cell for organic degradation.

It is interesting to note that reaction rate and the light emission of the corresponding solution as functions of frequency show a high similarity. Peaks are localised at the same frequencies and their relative proportions are similar for both phenomena. In other words, for a given transducer and cell geometry sonoluminescence and chemical activity of this type appear to be related. To confirm the correlation between sonoluminescence and chemical activity another reaction, oxidation of iodide into iodine, was performed.

5.2 Oxidation of iodide into iodine

5.2.1 Experimental scale

The set-up for the ultrasonic irradiation of iodide solutions was the same as in the case of the degradation of Meldola blue. However, contrary to Meldola blue and in spite of the brown coloration due to the production of triiodide, the reaction was not followed by spectrophotometry. The major reason for this change in experimental protocol was that oxidation of iodide does not follow first order kinetics, at least over a long period of time. Production of triiodide was found to be much more rapid during the first minute of irradiation. For these reasons and the fact that triiodide is electroactive, an electrochemical rate measurement protocol was adopted. This involved the employment of a flow cell and a pump to carry the reactants from the ultrasonic cell to the electrode.

In order to measure accurately the rate of I_3^- production it was necessary to calibrate the flow cell and pump respectively (see chapter 2 figures 2.15 and 2.16). The calibration of the peristaltic pump and the determination of the mass transfer coefficient under such experimental conditions were made with a degassed 5 mmol dm^{-3} hexaamine ruthenium (III) chloride, $[Ru(NH_3)_6]Cl_3$ (Strem Chemicals, 99 %), in a 0.1 mol dm^{-3} KCl electrolyte solution. For the highest flow rate of the pump, the steady state current for the Ru (III) reduction was found to be 8.17×10^{-8} A.

The corresponding mass transfer coefficient was determined from,

$$k_m = \left(\frac{i_{ss}}{nFSC} \right)$$

and hence for a flow rate of 5 ml min^{-1},

$$k_m = 0.215 \text{ cm s}^{-1}$$

As the diffusion coefficients for triiodide ($D = 9 \times 10^{-6}$ cm^2 s^{-1}) [18] and for $Ru(NH_3)_6^{3+}$ are very similar, the mass transfer coefficient of triiodide and ruthenium will be assumed to be equal for further calculations.

The irradiation of the solution is thought to provoke the oxidation of iodide in the following way [12],

$$3I^- + 2OH^{\cdot} \rightarrow I_3^- + 2OH^-$$

This was attributed to the formation of hydroxyl radicals from the dissociation of water, which is activated by transient cavitation.

In order to measure the rate of I_3^-, the reverse reaction was driven electrochemically. At the electrode surface,

$$I_3^- + 2e^- \Leftrightarrow 3I^-$$

and using the pump calibration the rate of I_3^- production was determined directly.

Figure 5.6 shows a linear increase in reduction current as a function of time after the first 25 seconds, (the time measured to drive the solution from the irradiation cell to the flow cell). Therefore, at a given irradiation frequency, the variation of the concentration in triiodide was determined using the initial slope of the current versus time plot and using the following expression:

$$\frac{dC}{dt} = \frac{1}{nFSk_m^{I_3^-}}\left(\frac{di}{dt}\right)$$

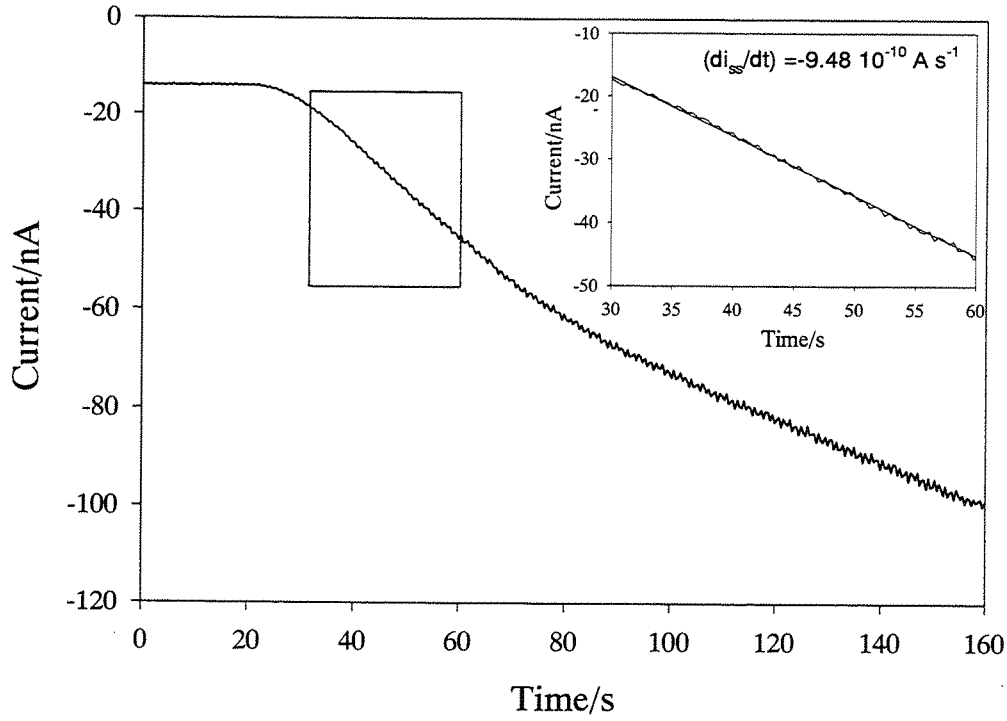

Figure 5.6: Plot showing the variation of the reduction current versus time recorded at a 0.5 mm Pt microelectrode. This current corresponds to the reduction of triiodide formed during the irradiation at 126.0 kHz of a 100 mmol dm^{-3} KI solution. The insert shows the part of curve used to calculate the initial slope. The plateau observed on the main graph corresponds to the time required by the solution to be pumped from the irradiation cell to the flow-cell.

From these measurements carried out at different frequencies, it was possible to obtain the frequency dependence of the reaction rate (figure 5.7). It can be seen that in general the rate measurement and sonoluminescence are correlated as functions of frequency.

Reproducibility of experiments was found to be non-ideal. However, it should be noticed that sonoluminescence measurements and first run of reaction rate determination were achieved in the same period of time, whereas the other runs of experiment were performed a few months later. Therefore a possible explanation of the poor reproducibility can be found in the modification of the external conditions that affect for example the concentration of dissolved impurities within the solution. Additionally each experimental run always produced the maximum rate within approximately 1 kHz of the sonoluminescence peak with only the absolute rate changing. This observation implies that the frequency dependence of the reaction remains the same while the absolute rate may be affected by other experimental factors.

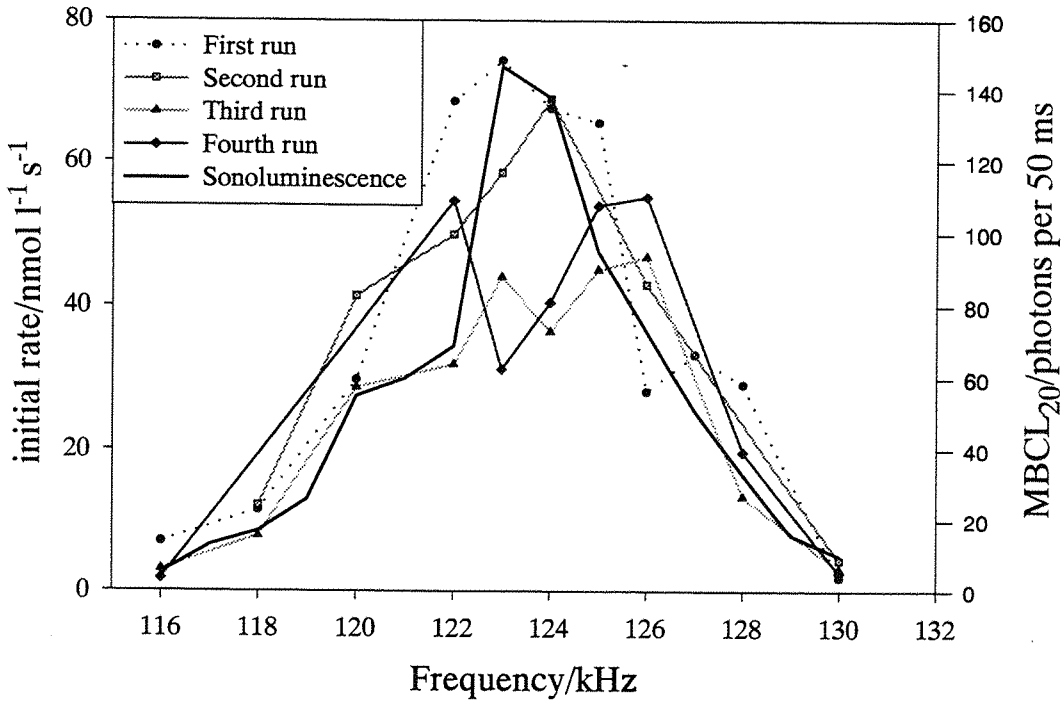

Figure 5.7: Degradation rate of a 100 mmol dm^{-3} KI solution as a function of applied ultrasound frequency. First run of measurements was carried out using a 10 mm Pt microelectrode as a working electrode, in the other runs 0.5 mm Pt electrode was used. Bold line represent sonoluminescence of a 0.1 mol dm^{-3} NaCl and 10 mmol dm^{-3} solution.

Weissler and his co-workers [12] found a degradation rate of 220 nmol s^{-1} at 1000 kHz and 300 Watts input. Rates were found to be much lower in the present work (figure 5.7) but the device employed and other experimental parameters such as frequency and input power were different.

5.2.2 Scale-up

To be used on an industrial scale, an ultrasonic device has to permit the treatment of large volumes of waste-water effluent. Moreover, the ultrasonic intensities have to be similar to those applied in the laboratory. In order to study the viability of the present device, larger volume of iodide solution were sonicated. As previously, initial degradation rate was followed during the irradiation of a 100 mmol dm^{-3} KI solution in the perspex cell. The sonicated volume was one litre.

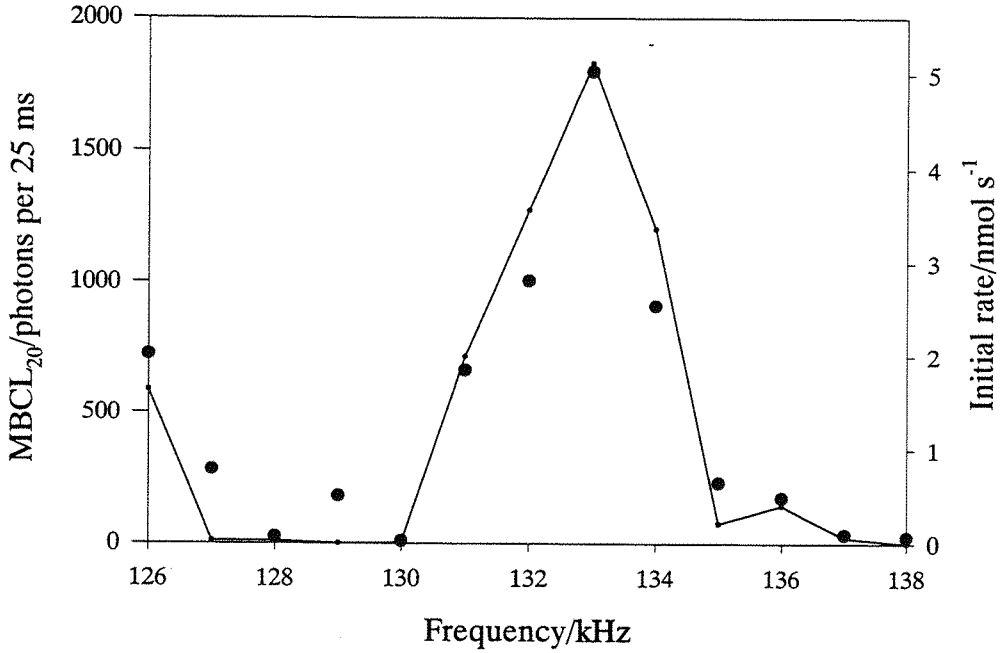

Figure 5.8: Sonochemiluminescence of a 1.2 mmol dm^{-3} luminol and 50 mmol dm^{-3} Na_2CO_3 solution (solid line) and degradation rate of a 100 mmol dm^{-3} KI solution (black points) as a function of the applied ultrasound frequency. The irradiation was carried out in a one litre cylindrical cell attached to a 33 kHz resonant frequency transducer.

Figure 5.8 shows a comparison of the sonochemiluminescence and oxidation rate of iodide as functions of the driving frequency. As shown previously, a preliminary study of the sonochemiluminescence allows prediction of the most efficient frequency to observe the degradation of any contaminant.

In sonoluminescence experiments, emission of photons was found to be the most effective at 133 kHz with an average of 1830 photons emitted per 25 ms for one litre of solution. In the case of the glass cell, maximum photons emission from 100 ml of solution was 4490 per 50 ms. Therefore, the highest sonochemiluminescence ratio of the glass cell to the perspex cell is per unit of volume:

$$\text{Sonochemiluminescence ratio} = \frac{\left(\dfrac{\text{photons emitted per 50 ms}}{\text{volume of solution}}\right)_{\text{glass cell}}}{\left(\dfrac{\text{photons emitted per 50 ms}}{\text{volume of solution}}\right)_{\text{perspex cell}}} = \frac{\dfrac{4490}{100}}{\dfrac{1830 \times 2}{1000}} = 12$$

The chemical activity ratio is:

$$\text{Chemical activity ratio} = \frac{(\text{best initial rate})_{\text{100ml experiments}}}{(\text{best initial rate})_{\text{scale-up experiments}}} = \frac{7.85e^{-8}}{5.03e^{-9}} = 16$$

These ratios are found to be very closed. In other words an ultrasonic device is all the more efficient to activate a chemical reaction since sonochemiluminescence per unit of volume of irradiated solution using this device is high.

From this observation and the comparison of the chemiluminescence emitted by a 100 ml with that of a one litre solution (see figure 4.7), it can be said that an increase of the sonicated volume provokes a loss of efficiency.

5.3 Conclusion

Sonochemiluminescence and degradation rates as function of frequency are correlated to each other. However, measurements of reaction rates are characterised by poor reproducibility because of the sentivity of the ultrasonic field to physical conditions.

References

[1] M. H. Entezari, P. Kruus, *Ultrasonics sonochemistry 3* (1996) 19.

[2] M. Gutierrez, A. Henglein, H. Moeckel, *Ultrasonics sonochemistry 2* (1995) 111.

[3] T. Kimura, T. Sakamoto, J. Leveque, H. Sohmiya, M. Fujita, S. Ikeda, T. Ando, *Ultrasonics sonochemistry 3* (1996) 157.

[4] A. Kotronarou, G. Mills, M. R. Hoffmann, *J. Phys. Chem 95* (1991) 3630.

[5] C. Petrier, M.-F. Lamy, *J. Phys. Chem. 98* (1994) 10514.

[6] S. Moon, L. Duchin, J. V. Cooney, *Tetrahedron letters 41* (1979) 3917.

[7] I. Hua, R. H. Hoechemer, M. R. Hoffmann, *J. Phys. Chem. 99* (1995) 2335.

[8] J. W. Chenand, W. M. Kalback, *I&EC Fundamentals 6* (1967) 175.

[9] D. S. Kristol, H. Klotz, R. C. Parker, *Tetrahedron letters 22* (1981) 907.

[10] A. Tuulmets, P. Raik, *Ultrasonics sonochemistry 6* (1999) 85.

[11] F. Trabelsi, H. Ait-Lyazidi, B. Ratsimba, A. M. Willhelm, H. Delmas, P.-L. Fabre, J. Berlan, *Ultrasonics sonochemistry 3* (1996) .

[12] A. Weissler, H. W. Cooper, S. Snyder, *J. Am. Chem. Soc.* (1950) 1769.

[13] M. R. Hoffmann, I. Hua, R. Hoechemer, *Ultrasonics sonochemistry 3* (1996) 163.

[14] M. H. Entezari, P. Kruus, *Ultrasonics sonochemistry 1* (1994) 75.

[15] C. Petrier, A. Jeunet, J.-L. Luche, G. Reverdy, *J. Am. Chem. Soc. 114* (1992) 3148.

[16] G. C. Topilskii, P. A. Egorov, L. V. Kortchaguin, *Ukrenia J. Chem. 8* (1967) 853.

[17] J. Berlan, F. Trabelsi, H. Delmas, A. M. Wilhelm, J. F. Petrignani, *Ultrasonics sonochemistry 1* (1994) 97.

[18] M. Bertotti, D. Pletcher, *Analytica Chimica Acta 337* (1997) 49.

6 Concluding remarks

6.1 General conclusions

The influence of the driving frequency on the electrical properties of the transducer, the pressure field within the cell and activity were investigated. Measurements of the physical and chemical activities were found to be strongly dependent on the driving frequency. A chemical reaction was found to be faster only at discrete frequencies which depend on the transducer and on the cell. Moreover, during sonochemiluminescent experiments, chemical activity was observed to be much more enhanced at frequencies where a standing wave pattern was visible.

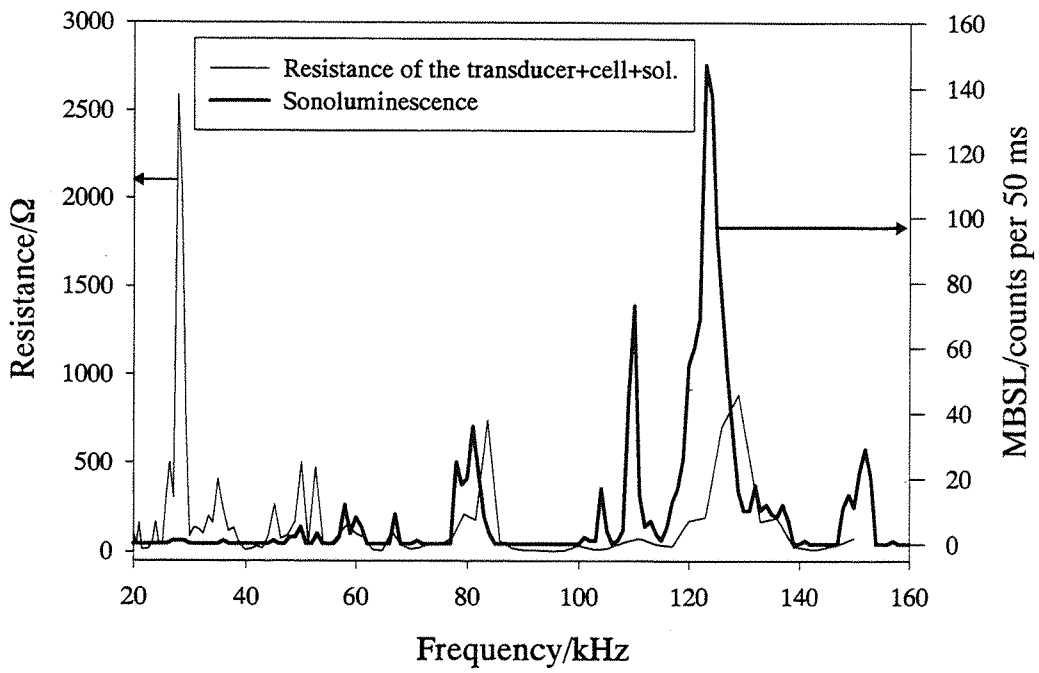

Figure 6.1: Comparison of the transducer resistance and sonoluminescence as functions of frequency. Measurements were achieved during the irradiation of a 100 ml solution containing 0.1 mol dm^{-3} NaCl and 10 mmol dm^{-3} HCl.

Figure 6.1 shows a comparison of the transducer resistance and sonoluminescence of a 100 ml solution containing 0.1 mol dm^{-3} NaCl and 10 mmol dm^{-3} HCl as functions of frequency. Peaks of light emission correspond to a modification of

the transducer properties. However, for both measurements efficient frequencies are found to be very similar, although the relative magnitudes of the peaks are completely different. Maximum impedance change occurs at low frequencies (≤ 80 kHz), whereas light emission is more efficient at high frequencies (>80 kHz).

The acoustic field within a cell determines the presence and the nature of cavitation events. Moreover, sonoluminescence and sonochemistry are thought to be directly related to cavitation. Therefore it seems logical to correlate activity within a cell to the pressure field. However, the present results prove that this inference is not so simple.

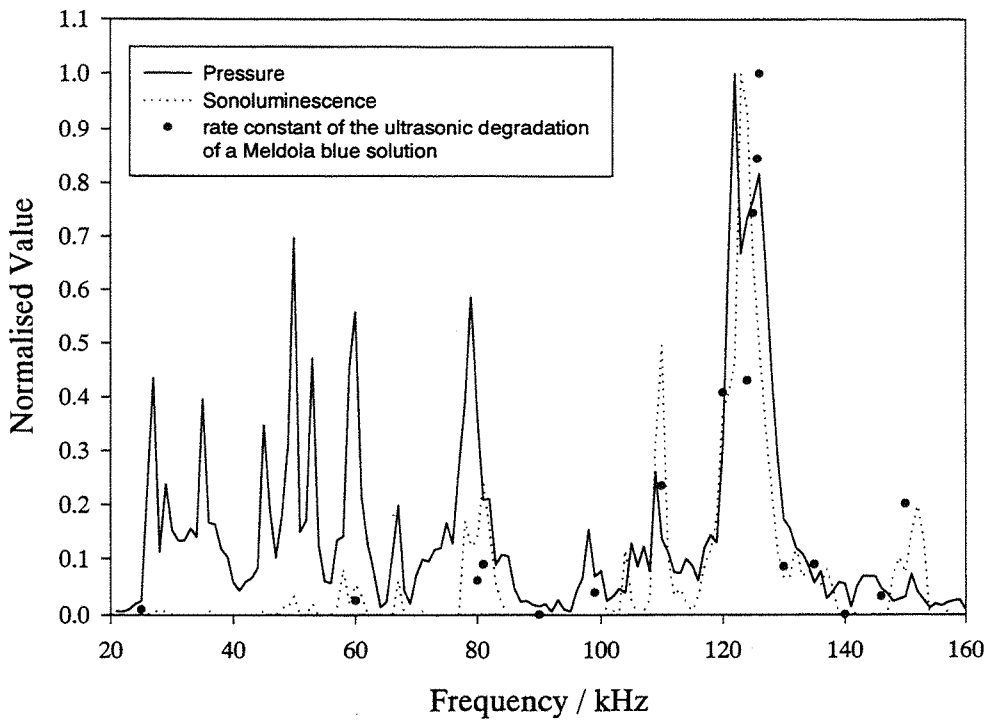

Figure 6.3: Comparison of the sonoluminescence, rate of reaction and a local measurement of the pressure within the cell as functions of frequency. Pressure and luminescence measurements were achieved during the irradiation of a 10 mmol dm^{-3} HCl and 0.1 mol dm^{-3} NaCl solution and for the same height of solution in the cell (even in the presence of the hydrophone). Solutions of Meldola blue also contain 10 mmol dm^{-3} HCl and 0.1 mol dm^{-3} NaCl.

As shown on figure 6.3, a plot of pressure measurement versus frequency does not reflect the chemical reactivity of the irradiated system as well as sonoluminescence

does. At low frequencies (< 80 kHz) chemical activity and luminescence are found to be inefficient whereas high pressure peaks are observed in this region. One possible explanation is that pressure measurements are local and do not give an indication of the whole solution. The second hypothesis is that the process of cavitation itself changes. However, the second explanation appears less likely as it should be noted that all the measurements (luminescence, pressure field and reaction rate) were carried out with solutions having the same physical properties (viscosity and speed of sound).

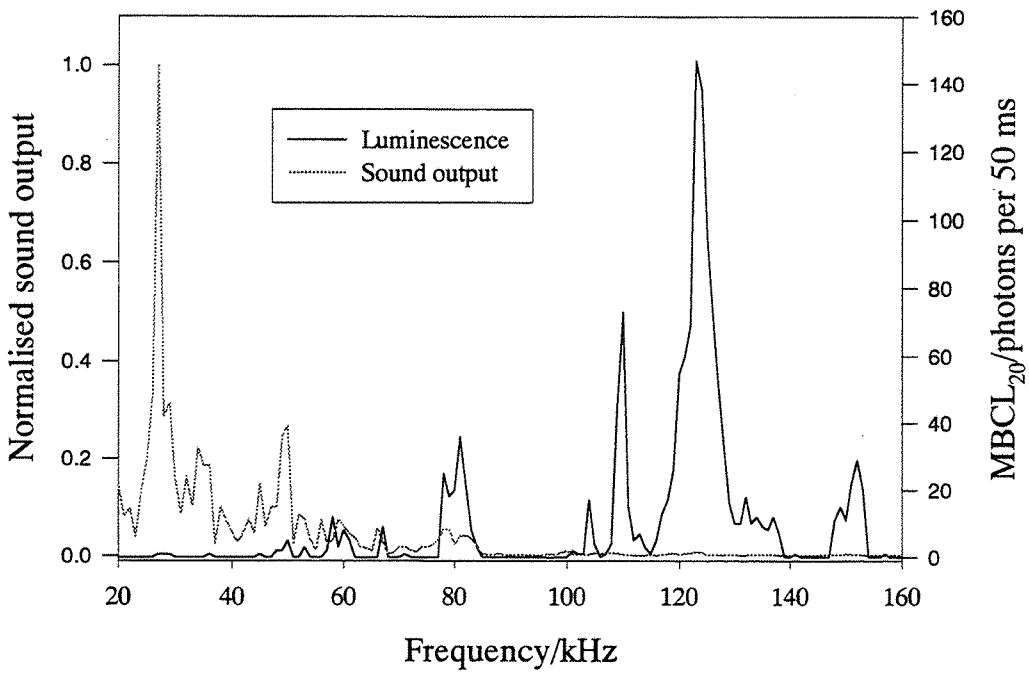

Figure 6.4: Comparison of the sound output (from 20 Hz to 20 kHz) and light emission from a sonicated solution containing 10 mmol dm^{-3} HCl and 0.1 mol dm^{-3} NaCl as function of the driving frequency. 100 ml of this solution was irradiated in a cylindrical glass cell

As seen in figure 6.4 the sound output from a sonicated solution as a function of the driving frequency seems to give some indication of the corresponding chemical activity. However, conclusions from this comparison are limited. The frequency bandwidth limitations from the microphone could explain this bad correlation between luminescence and sound emission. Nevertheless, the observation that audible sound does not appear to predict chemical activity still stands.

Chemical activity and sonochemiluminescence were found to be correlated to each other. Therefore a preliminary study on the light emission from an alkaline luminol solution appears to be an easy and convenient method to characterise the best conditions of irradiation. Moreover, such a study allows the chemical active zones within a reactor to be mapped. For a cylindrical reactor, characteristic patterns exist. These consist of equidistant bands on vertical views of the cell and circles from a top of the cell view. Such observations are consistent with a standing wave pattern.

6.2 Further work

Pressure measurements were not achieved at a particular position within the cell. At a certain frequency this position could correspond to a pressure antinode, and at another frequency this point would not be at a special position of the sound field. Therefore it would be interesting to study the pressure at the surface of the transducer which is a pressure antinode for all the frequencies. Such a measurement cannot be achieved with the same type of hydrophone used in this work because the acoustic centre of the hydrophone is surrounded by other materials. Therefore direct contact between the transducer and the sensitive part of the hydrophone was not possible. On the other hand a measurement of the motion of the transducer surface by a piezoelectric material attached to its surface is feasible and proportional to surface motion. The glass cell cannot be used for this type of experiment since the transducer is attached to the cell and is not a part of the cell itself but this is not the case in the perspex cell.

Hydrolysis of an ester should be achieved to complete the set of studied reactions. Such a reaction is all the more interesting since the mechanism is very simple.

It will be also interesting to carry out the same kind of general study for different cell geometries.

As seen previously a relatively bad correlation between audible sound output and light emission from the same sonicated solution was found. In order to improve this comparison of the sound output for higher frequency (>20 kHz) should be performed.

Appendix: Calculation of the absorbance during the ultrasonic degradation of Meldola blue

When samples are taken (see chapter 5.1.2), the same volume of electrolyte was added to keep the volume of the sonicated solution constant. Hence, any variation in Meldola blue concentration is due to the ultrasonic degradation but also to the successives dilutions. The aim of this appendix is to determined the contribution of dilution to the modification of absorbance.

After the first dilution, the concentration of Meldola blue in the cell, $[M]_2$, is determined by the following equation:

$$[M]_2 \times V_{sol} = [M]_1 \times (V_{sol} - V_{sample})$$

where $[M]_1$, V_{sol}, V_{sample} represent the initial concentration of Meldola blue, the volume of the solution and the volume of a sample.

hence,

$$[M]_2 = [M]_1 \times \frac{V_{sol} - V_{sample}}{V_{sol}}$$

In the same way after the second dilution, the concentration of Meldola blue in the cell, $[M]_3$, is:

$$[M]_3 \times V_{sol} = [M]_2 \times (V_{sol} - V_{sample})$$

hence,

$$[M]_3 = [M]_2 \times \frac{V_{sol} - V_{sample}}{V_{sol}} = [M]_1 \times \left(\frac{V_{sol} - V_{sample}}{V_{sol}}\right)^2$$

After the n^{th} dilution the concentration of Meldola blue in the cell, $[M]_n$, is:

$$[M]_n = [M]_{n-1} \times \frac{V_{sol} - V_{sample}}{V_{sol}} = [M]_{n-2} \times \left(\frac{V_{sol} - V_{sample}}{V_{sol}}\right)^2 = \ldots = [M]_1 \times \left(\frac{V_{sol} - V_{sample}}{V_{sol}}\right)^{n-1}$$

The Beer Lambert law gives the absorbance as a function of concentration:

$$A = \varepsilon \times l \times C$$

where A, ε, l, C represent the absorbance of the solution, the extinction coefficient, the cuvette length and the concentration of the solution.

Supposing that the solution is not sonicated, after n dilutions, the measured absorbance is:

$$A_n^{measured} = \varepsilon \times l \times [M]_n = \varepsilon \times l \times [M]_1 \times \left(\frac{V_{sol} - V_{sample}}{V_{sol}} \right)^{n-1}$$

To take into account modification of absorbance due to dilution the measured absorbance should be multiplied by the following factor:

$$A_n^{modified} = \frac{A_n^{measured}}{A_{without\ dilution}} = A_n^{measured} \times \left(\frac{V_{sol}}{V_{Sol} - V_{sample}} \right)^{n-1}$$